Functional mapping in the human brain using high magnetic fields

Kâmil Uğurbil, Xiaoping Hu, Wei Chen, Xiao-Hong Zhu, Seong-Gi Kim and Apostolos Georgopoulos

Center for Magnetic Resonance Research, University of Minnesota, 2021 6th Street SE, Minneapolis, MN 55455, USA

An avidly pursued new dimension in magnetic resonance imaging (MRI) research is the acquisition of physiological and biochemical information non-invasively using the nuclear spins of the water molecules in the human body. In this trial, a recent and unique accomplishment was the introduction of the ability to map human brain function non-invasively. Today, functional images with subcentimetre resolution of the entire human brain can be generated in single subjects and in data acquisition times of several minutes using 1.5 tesla (T) MRI scanners that are often used in hospitals for clinical purposes. However, there have been accomplishments beyond this type of imaging using significantly higher magnetic fields such as 4 T. Efforts for developing high magnetic field human brain imaging and functional mapping using MRI (fMRI) were undertaken at about the same time. It has been demonstrated that high magnetic fields result in improved contrast and, more importantly, in elevated sensitivity to capillary level changes coupled to neuronal activity in the blood oxygenation level dependent (BOLD) contrast mechanism used in fMRI. These advantages have been used to generate, for example, high resolution functional maps of ocular dominance columns, retinotopy within the small lateral geniculate nucleus, true single-trial fMRI and early negative signal changes in the temporal evolution of the BOLD signal. So far these have not been duplicated or have been observed as significantly weaker effects at much lower field strengths. Some of these high-field advantages and accomplishments are reviewed in this paper.

Keywords: fMRI; BOLD contrast; human brain imaging; functional mapping; brain function

1. INTRODUCTION

The phenomenon of nuclear magnetic resonance (NMR) was described in landmark papers over 50 years ago (Rabi *et al.* 1938, 1939; Purcell *et al.* 1945; Bloch *et al.* 1946). Because of its ability to obtain discrete resonances sensitive to the chemical environment, NMR rapidly evolved to become an indispensable tool in chemical and biological research focused on molecular composition, structure and dynamics. In 1973, a novel concept using NMR of the hydrogen atoms in the human body as an imaging modality was introduced (Lauterbur 1973). While all NMR applications of the time were singularly concerned with eliminating inhomogeneities in magnetic field magnitude over the sample, this new concept embraced them and proposed using them to extract spatial information. From this early concept emerged magnetic resonance imaging (MRI) which is now solidly established as a non-invasive technique which permits the visualization of human anatomy with high spatial resolution and the ability to distinguish different types of tissues.

An avidly pursued new dimension in MRI research is the acquisition of physiological and biochemical information non-invasively using the nuclear spins of the water molecules in the human body. In this trial, a recent and unique accomplishment was the introduction of the ability to map human brain function non-invasively. The first functional image of the human brain was based on measurements of task-induced blood volume change assessed by intravenous bolus injection of an exogenous MRI contrast agent, a highly paramagnetic substance, into the human subject and tracking the bolus passage through the brain with consecutive, rapidly acquired images (Belliveau *et al.* 1991). However, this method was quickly rendered obsolete with the introduction of totally non-invasive methods of functional MRI (fMRI) of the brain (e.g. Bandettini *et al.* 1992; Kwong *et al.* 1992; Ogawa *et al.* 1992; Edelman *et al.* 1994; Kim 1995). These new methods permitted examination of functional specialization in the human brain with unprecedented spatial resolution.

Historically, one of the earliest compelling arguments for the existence of regional specialization of human brain function was presented by Broca (1855) in the middle of the 19th century. Broca (1855) examined a patient who was unable to speak as a result of a stroke but who was otherwise normal. Based on an autopsy performed subsequent to the patient's death, Broca & Brown-Sequard (1855) concluded that the seat of the damage was an egg-sized lesion located in the inferior frontal gyrus of the frontal lobe in the left hemisphere; this general area is now commonly referred to as Broca's area although its precise topographical extent remains ambiguous. This type of lesion study and later intra-operative mapping efforts with electrodes were, until

recently, the primary source of our current understanding of functional compartmentation in the human brain.

The language area first identified by Broca & Brown-Sequard (1855) can now be visualized with previously unavailable spatial resolution and detail using fMRI in data collection times that last only a few minutes. Figure 1 displays the three-dimensional (3D) result of such a study (P. Erhard, P. Strick, J. Strupp, A. K. Helms Tillery, S. Naeve-Velguth and K. Ugurbil, unpublished results). The grey-scale picture is an anatomical image. Superimposed onto the anatomical image in colour is the functional map generated during a covert task where the subjects were shown pictures of objects and were asked to name them. The left and right sides of the brain are seen in figure 1*a*,*b*. Figure 1*c* illustrates the 3D image from a different angle, looking onto the left side and the top of the brain. In these images, we see only the activation on the outer cortical surface. When the anatomical image is rendered partially transparent, activation in the interior of the brain and within its numerous folds (sulci) also becomes visible, albeit with diminished intensity (figure 1*d*).

These images are based on blood oxygen level dependent (BOLD) contrast, which was first described by Ogawa & Lee (1990) and Ogawa *et al.* (1990*a*,*b*) in rat brain studies and subsequently applied to generate functional images in the human brain (Bandettini *et al.* 1992; Kwong *et al.* 1992; Ogawa *et al.* 1992). BOLD contrast originates from the intravoxel magnetic field in homogeneity induced by paramagnetic deoxyhaemoglobin sequestered in red blood cells, which in turn are compartmentalized within the blood vessels. Magnetic susceptibility differences between the deoxyhaemoglobin-containing compartments versus the surrounding space devoid of this strongly paramagnetic molecule generate magnetic field gradients across and near the boundaries of these compartments. Therefore, signal intensities in magnetic resonance images sensitized to BOLD contrast are altered if the regional deoxyhaemoglobin content is perturbed. This occurs in the brain because of the spatially specific metabolic and haemodynamic response to enhanced neuronal activity; it has been suggested that regional blood flow (CBF) increases while the oxygen consumption rate ($CMRO_2$) in the same area is not elevated commensurably (Fox & Raichle 1986; Raichle 1987; Fox *et al.* 1988), resulting in a decreased extraction fraction and lower deoxyhaemoglobin content per unit volume of brain tissue. Consequently, the signal intensity in a BOLD-sensitive image increases in regions of the brain engaged by a 'task' relative to a resting, basal state.

BOLD contrast relies on the interplay between CBF and $CMRO_2$ as well as blood volume (CBV). As such, it represents a complex response controlled by several parameters (Ogawa *et al.* 1993, 1998; Kennan *et al.* 1994; Weisskoff *et al.* 1994; Boxerman *et al.* 1995*b*; Buxton & Frank 1997; Van Zijl *et al.* 1998). However, recent MRI techniques can also generate images based on quantitative measures of CBF changes coupled to neuronal activity (Kwong *et al.* 1992; Edelman *et al.* 1994; Kim 1995; Kim & Tsekos 1997; Kim & Ugurbil 1997; Wong *et al.* 1998). These CBF methods rely on tagging the blood spins differentially within and outside of a well-defined volume. For example, in the flow-sensitive alternating inversion recovery (FAIR) technique (Kim 1995; Kim & Tsekos 1997; Kim & Ugurbil 1997), frequency-selective inversion pulses are used to invert the longitudinal magnetization within a 'slab' along one direction (typically axial); in the absence of blood flow, the spins relax back to thermal equilibrium only by spin-lattice relaxation mechanisms characterized by the time constant T_1. If flow is present, however, the relaxation becomes effectively faster as unperturbed spins outside the inverted slab flow in and replenish the net magnetization within the slab. Consequently, the effective spin-lattice relaxation in FAIR, as well as in other flow-sensitive techniques (Detre *et al.* 1992, 1994; Roberts *et al.* 1994; Kim 1995; Kwong *et al.* 1995), becomes characterized by a shorter time constant T_1^*, which is related to blood flow. It also follows naturally that, if the inversion pulse in FAIR does not define a slab but inverts everything in the whole body (i.e. it is non-selective), blood flow does not enter into the problem at all. Thus, in the FAIR technique two images are acquired consecutively, each after a fixed delay period subsequent to the inversion pulse; in one the inversion pulse is slab selective and in the other it is non-selective. The difference image generated from this pair is a flow-sensitive image. Figure 2 illustrates the results of such a 'blood flow'-based functional imaging study in the human brain acquired at 4 tesla (T) during a finger movement task. The grey-scale image depicts CBF which is high in the 'grey' matter areas that contain the cell bodies and the dendrites and low in the white matter which is primarily composed of axons connecting the neurons. As expected, these CBF images resemble anatomical images that distinguish the grey and white matter in the brain. However, in the case of the blood flow image illustrated in figure 2, the signal intensity can be quantitated and assigned a number in terms of millilitres of blood delivered per minute to a gram of brain tissue (Kim 1995; Kim & Tsekos 1997). The colour map describes regions in the brain where blood flow increased in response to the execution of the finger movement task; this is the 'activation' or 'functional' image. Note the excellent correspondence between the colour map and the grey matter areas in figure 2; this is expected from a good functional image at this spatial resolution and is evidence of the accuracy of these maps because blood flow is high to begin with and increases more in the grey compared to the white matter during elevated neuronal activity.

2. UNIQUE ACCOMPLISHMENTS IN fMRI AT HIGH MAGNETIC FIELDS

Today, images like those shown in figure 1 can be generated by 1.5 T scanners that are often found in hospitals, provided the scanner is equipped with the appropriate hardware to perform fast imaging. These are relatively 'low' resolution images in the several millimetre spatial domain obtained by averaging many executions of the same task by a single individual. However, there have been accomplishments beyond this type of imaging using significantly higher magnetic fields than 1.5 T.

Shortly before the introduction of BOLD-based fMRI, efforts were initiated in three laboratories (the Universities of Minnesota and Alabama and the National Institutes of Health) to explore the possibility of using

high magnetic fields (4 T) for human MRI. However, these high-field ambitions were met with scepticism and the possibility of human imaging at magnetic fields much higher than 1.5 T was seriously questioned. This scepticism was not based on the existence of any experimental evidence; rather, it followed from concepts and theoretical considerations regarding the interaction of high-frequency electromagnetic waves with the conductive human body. These considerations led prominent investigators in the field of MRI research to suggest as early as 1979 that human imaging would not be possible beyond 10 MHz (*ca.* 0.24 T) (Hoult & Lauterbur 1979). Of course, even clinical imaging is now performed at magnetic fields much higher than 0.24 T, and recent work at 3 and 4 T has demonstrated that exquisite anatomical and functional imaging of the human head is achievable at these high fields.

In our laboratory, the trial with high magnetic fields coincided with the focus on developing BOLD-based fMRI and all fMRI studies, including the first paper from our group (Ogawa *et al.* 1992), were conducted at 4 T. The fMRI advantage comes from the fact that the 'extravascular' BOLD response (i.e. the contribution to the transverse relaxation rate (R_2^*) of nuclear spins in the presence of deoxyhaemoglobin compartmentalized in a cylinder approximating a blood vessel) is expected to behave according to the equations (e.g. Boxerman *et al.* 1993; Ogawa *et al.* 1993, 1998; Weisskoff *et al.* 1993)

$$R_2^* = \alpha\{\Delta\chi_O\omega_O(1-Y)\}b_{vl} \text{ (large blood vessels)}, \quad (1)$$

and

$$R_2^* = \eta\{\Delta\chi\omega_O(1-Y)\}^2 b_{vs}p \text{ (small blood vessels)}, \quad (2)$$

where $R_2^* = 1/T_2^*$, α and η are constants, ω_O is the external magnetic field in frequency units (rad s^{-1}), $\Delta\chi_O$ is the maximum susceptibility difference expected in the presence of fully deoxygenated blood, Y is the fraction of oxygenated blood present, $\{\Delta\chi_O\omega_O(1-Y)\}$ is the frequency shift due to the susceptibility difference between the cylinder simulating the deoxyhaemoglobin-containing blood vessel, b_{vl} is the blood volume for large blood vessels (veins and venuoles with a radius greater than *ca.* 5 μm for 4 T), b_{vs} is the small vessel blood volume (capillaries and small post-capillary venuoles, less than *ca.* 5 μm in radius) and p is the fraction of active small vessels (i.e. filled with deoxyhaemoglobin-containing red blood cells). An important feature of equation (2) is the fact that it varies as the square of the external magnetic field for small blood vessels where the effect is dominated by dynamic averaging. In contrast, the dependence on the external magnetic field is linear for large blood vessels. The improved contrast that comes from the increased magnetic field and the elevated sensitivity to small blood vessels provide advantages. However, it has been argued that high magnetic fields also result in elevated image-to-image signal fluctuations which effectively reduces the contrast-to-noise ratio in the functional images. This has not been experimentally demonstrated; in contrast, comparison studies have shown that the contrast-to-noise ratio increases with the magnetic field strength up to 4 T, the highest field studied at the time (Gati *et al.* 1997). Furthermore, it has been clearly demonstrated that image-to-image fluctuations can be suppressed in fMRI data (Hu & Kim 1994; Hu *et al.* 1995; Mitra *et al.* 1995, 1997; Biswal *et al.* 1996; Ogawa *et al.* 1996). Ultimately, one must consider the presence of accomplishments at high magnetic fields that have not been duplicated at much lower field strengths. The rest of this paper will review some of these advantages and accomplishments.

(a) *Single-trial fMRI*

Most fMRI studies use a 'block' design where periods of a 'control' state are interleaved with periods of task performance and/or sensory stimulation. The control period itself may also require the subject to perform a task and/or be subjected to sensory stimulation. The images are generated by examining the difference between the control and the task periods. Each of these periods are relatively long, typically 1 min or longer and the subject executes the task many times. The picture that emerges from such a study is a time average which 'blurs' important information regarding the temporal evolution of the neuronal activity in different parts of the brain. Equally important, cognitive effects such as learning, alteration in strategy, etc., which evolve with repeated executions, are also averaged into the final image generated.

fMRI is actually a real-time measurement. Single-slice fMRI images can be acquired in tens of milliseconds, which is adequate for monitoring neuronal responses. Unfortunately, the temporal response of fMRI signals is dictated by the response of the vascular system which is characterized by a time constant of seconds. This was demonstrated in one of the early fMRI studies (Blamire *et al.* 1992) and subsequently confirmed in numerous other reports (e.g. Savoy *et al.* 1995; Hu *et al.* 1997; Kim *et al.* 1997; Richter *et al.* 1997*a*,*b*; Menon *et al.* 1998). However, even within this temporal regime, useful information on brain function can be obtained since there exist numerous tasks and processes that necessarily engage the human brain for prolonged periods. In this temporal domain, signal changes in the fMRI images track the temporal evolution of stimulation or mental task performance very well, albeit with a shift in time or a delay that lasts several seconds. This capability permits the acquisition of fMRI data gated to a particular time point in stimulus onset or instruction–execution sequence. In either case, this type of fMRI data collection is referred to as event-related fMRI.

In event-related fMRI, two distinct types of experiments have been performed. Buckner *et al.* (1996) acquired images gated to the onset of a task in a paradigm so that the temporal evolution of the fMRI signal during and following the execution of the task could be temporally co-registered and averaged following repeated executions of the same task. However, such averaging loses unique information associated with each execution of the task; subjects do not perform the same way each time as both brain function and performance are modulated by effects which come into play, such as learning, alterations in strategy, errors and habituation. In addition, when averages of single trials are performed, it is not possible to conclude much about the temporal differences that may be observed between different regions of the brain; such a difference was reported in the

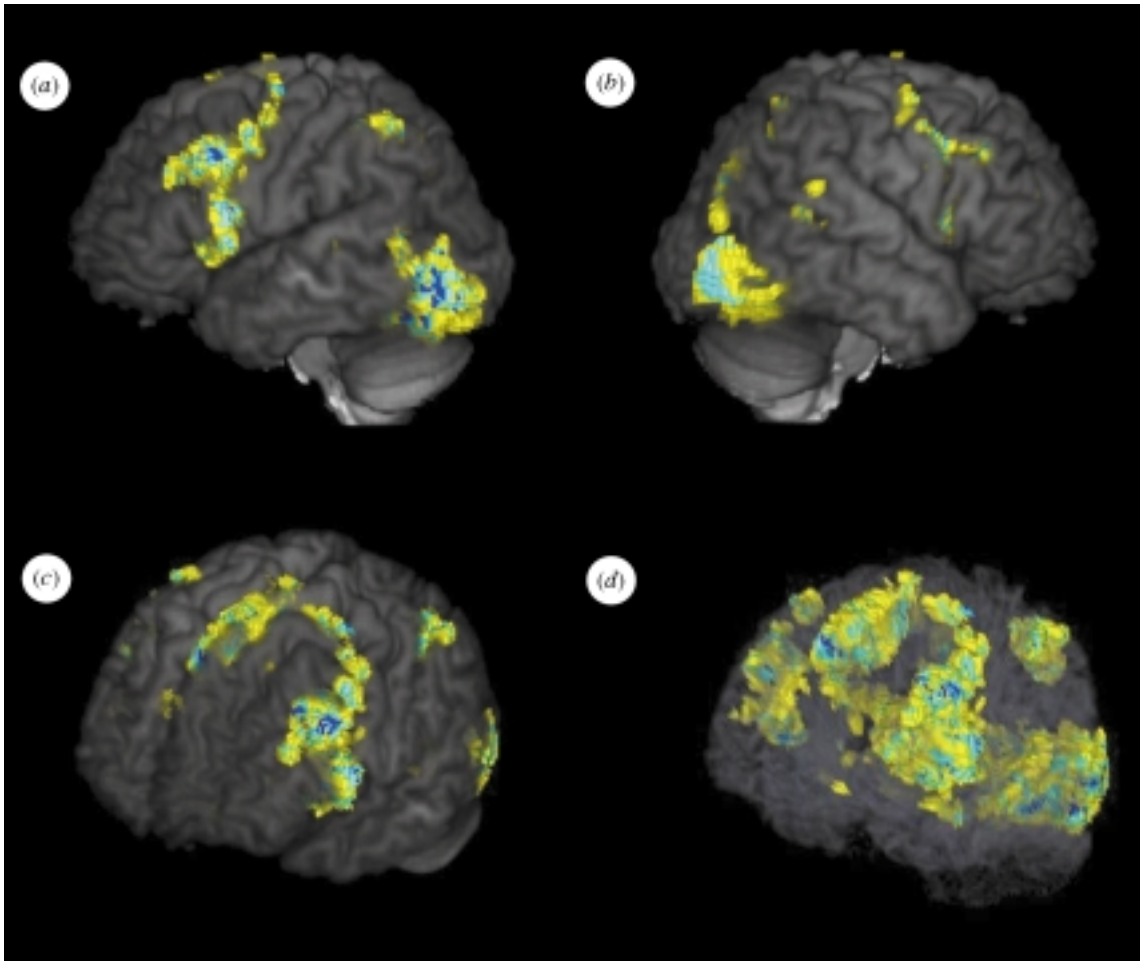

Figure 1. Three-dimensional, whole brain images of activation during a language task based on word generation from a phoneme. Subjects were presented phonemes and were asked to think of as many English words as they could that contained the phoneme until the presentation of the next phoneme. We are looking at the brain either from a view where we see (*a*) the left or (*b*) the right hemispheres or (*c*) from an angle where the left hemisphere and top of the brain are both partially visible. The extensive frontal cortex activity depicted in (*a*) largely defines the area of Broca and extends to area 46 as well. In (*a–c*) the anatomical images are opaque; consequently, only activated regions that lie predominantly on the cortical surface are seen. (*d*) is identical to (*c*) except that the anatomical image was rendered partially transparent so as to be able to effectively 'look through' and see the activated regions that would normally be blocked from view by the overlapping cortex (e.g. regions within the sulci). In these particular views, activity in the medial part of the brain and other areas are also apparent, albeit, with diminished intensity.

study by Buckner *et al.* (1996) where activation in left prefrontal areas involved in language were delayed *ca.* 2 s relative to extrastriate areas during a word generation task. Of course, the human brain performs this task much faster than 2 s and this time difference cannot really be attributed to differences in brain activation. Rather, one must conclude that differences in the haemodynamic response of the fMRI signal in different regions of the brain exist. However, in this study this distinction cannot be made from the data alone and the interpretation of the results would be ambiguous in less obvious cases when this approach is used.

The second type of experiment was a true single-trial fMRI study achieved with the use of high magnetic fields, namely 4 T (Kim & Richter 1996; Richter & Kim 1996; Richter *et al.* 1996, 1997*a*,*c*; Kim *et al.* 1997). Intentionally and specifically, it was demonstrated that, at least at 4 T, there exists enough sensitivity to monitor fMRI signal evolution in a single execution of a task without averaging over many trials. This point is important. With this capability, it is then possible to perform many such single-trial executions of a task and not average them but store them separately and subsequently analyse and correlate the fMRI data with differences in aspects of the subject's performance (e.g. response time, errors, etc.). In this way, the haemodynamic response time differences can also be factored out and distinguished from the temporal behaviour of neuronal activity. An alternative approach is to average such single trials, but using performance or response criteria, pooling together only those responses that are similar.

An example of a true single-trial study conducted at 4 T monitoring the evolution of fMRI signals in the human brain before, during and subsequent to an instruction and the execution of a motor task is illustrated in figure 3. EMG recording and single-trial fMRI signal intensity time-courses in motor areas for a single subject are displayed in this figure. The EMG recording is shown in the bottom trace. M1 represents the contralateral primary motor area, PM the bilateral premotor

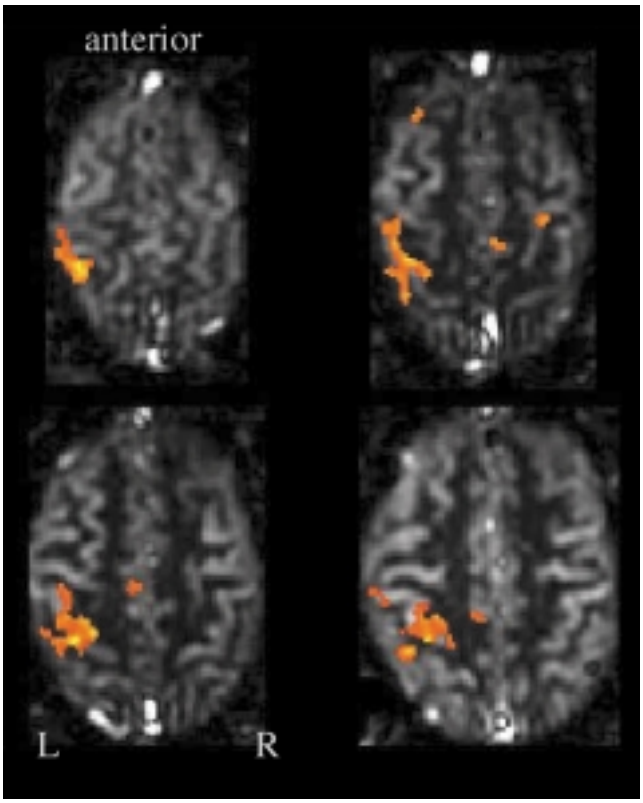

Figure 2. Multislice study of finger opposition task examined with the FAIR technique measuring blood flow changes (Kim & Tsekos 1997). The grey-scale image depicts signal intensity proportional to blood flow. The colour map identifies regions of the brain where blood flow changed during the tasking period. Note the excellent correspondence of the colour map with grey matter areas identified by the higher intensity regions in the grey-scale map. Grey matter has higher blood volume and blood flow than white matter. Consequently, the FAIR images have higher intensity in the grey matter areas.

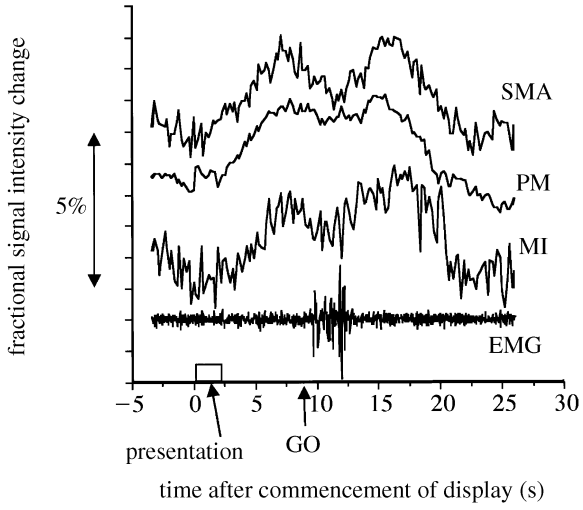

Figure 3. Single-subject, single-trial fMRI (without averaging) time-courses in three regions of the brain together with EMG recording of muscle movement during a visually instructed delayed finger movement task. From Richter & Kim (1996) and Richter *et al.* (1997*a*). For abbreviations, see text.

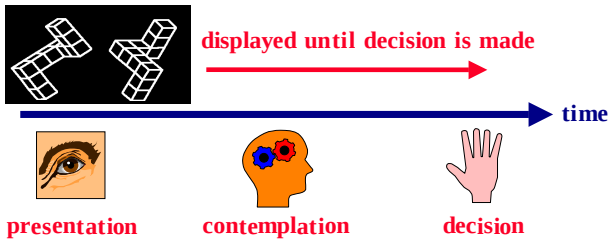

Figure 4. The paradigm in the true single-trial 'mental rotation' study by Richter *et al.* (1997*b*).

area and SMA the bilateral supplementary motor area. The task is a visually instructed, delayed, cued, four-finger movement; in this trial the presentation starts at $t=0$ and lasts for 2.1 s and the GO signal for task execution is displayed at $t=9.1$ s. The EMG shows no movements during the motor preparation period between instruction and GO. Activation of the primary (M1) motor area as well as supplementary and premotor areas is observed during motor execution and preparation. These data are virtually identical to electrode recordings taken from the same areas of monkey cortex during execution of the same task, except that the fMRI data are displaced in time by seconds relative to the actual time of neuronal activity. The data presented in figure 3 also illustrate the sensitivity of the high-field fMRI method. Like the electrode recordings from primates, in this task the fMRI data demonstrate that the primary motor cortex is active during the motor preparation period. However, this has been a controversial issue with humans because positron emission tomography (PET) studies did not reveal activation during such motor preparation (Decety *et al.* 1992). In the high-field fMRI study, this activation is detectable in a single execution of the task.

This type of true single-trial experiment was also used to correlate aspects of activation with task performance (Richter *et al.* 1997*a*,*c*). The paradigm employed was the 'mental rotation' task of Shepard & Metzler (1971). The subjects were presented with drawings of 3D objects, examples of which are illustrated in figure 4. In each task, a pair of objects was presented; they were either identical or mirror images and they were rotated relative to each other through varying degrees. The subject had to identify whether the pair was identical or a mirror image and report it by pressing one of two buttons. In this task, the subject's response time depends on the angle through which the two objects are rotated relative to each other. The experiment started with the subject looking at similar but identical 3D objects. When ready, the subject commenced the scanning process by pressing a button. The 3D objects were shown and the subject made a decision; after a suitable delay to allow for the haemodynamic response to return to basal levels, the process was repeated. Figure 5 displays signal intensity curves from the parietal lobe from two trials where the response time of the subject was different. The width of the response was evaluated for a correct response only with respect to the response time. In each individual, a linear correlation was found (figure 6). However, the intercept corresponding to a response time of zero was significantly different for the different individuals, presumably

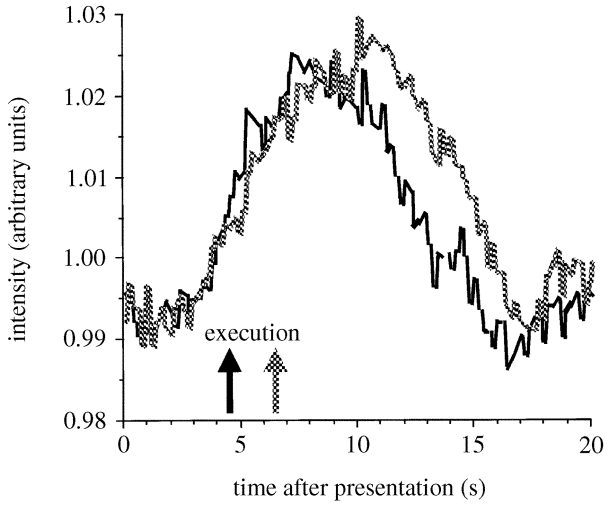

Figure 5. The T_2^*-weighted BOLD response in the parietal lobe for two different single trials (no averaging) for the paradigm outlined in figure 4. The arrows indicate the time at which the subject responded. From Richter *et al.* (1997*b*).

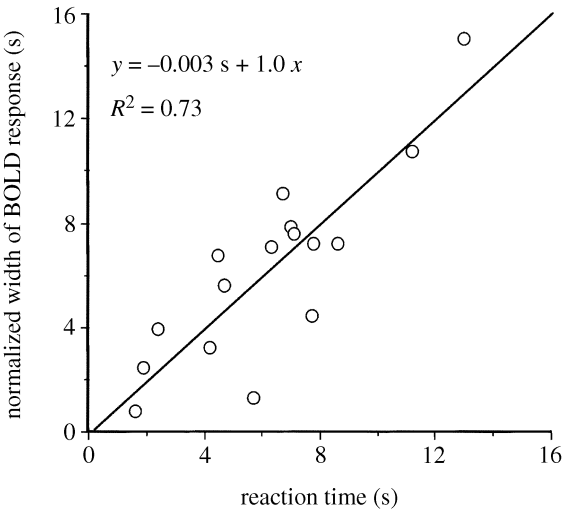

Figure 7. The width of the fMRI response (figure 5) versus performance data from all subjects subsequent to removal of the time zero intercept. Each point represents a true single trial in a single subject (no averaging). From Richter *et al.* (1997*b*).

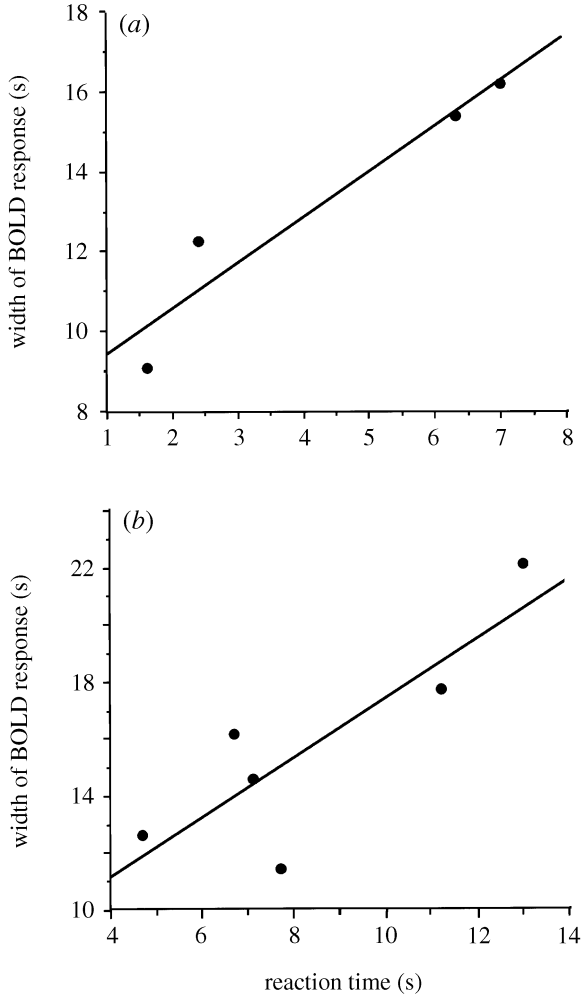

Figure 6. fMRI versus performance data from two different subjects. The correlation between the width of the fMRI time-course and subject response time extracted from the single-trial study where data and images were acquired from each individual trial and correlated with performance at the end of the study. From Richter *et al.* (1997*b*).

reflecting fundamental differences in the haemodynamic response to elevated neuronal activity among individuals. When this subject-dependent variable was subtracted out, each single-trial, single-subject data point for all subjects yielded excellent correlation with the response time (figure 7).

One potential confounding problem with such signal trial fMRI studies is the presence of various types of spatio-temporal patterns in the fMRI signals even under basal 'resting' conditions. T_2^*-weighted MRI signals fluctuate with heart beat and respiration; however, such fluctuations can be removed from the fMRI data (e.g. Hu & Kim 1994; Hyde *et al.* 1994; Hu *et al.* 1995; Mitra *et al.* 1995, 1997; Biswal *et al.* 1996). When cardiac and respiratory fluctuations are suppressed, the fMRI signal from the resting human brain still exhibits low frequency oscillations at *ca.* 0.1 Hz (Biswal *et al.* 1995, 1997; Ogawa *et al.* 1996; Mitra *et al.* 1997). Near-infrared optical studies also show this slow oscillation. Therefore, techniques that can separate the fMRI data into its various components (e.g. Mitra *et al.* 1997) and in the process significantly improve the effective signal-to-noise ratio for detection of function will play a crucial role in mapping brain function, particularly in single-trial fMRI studies with temporal resolution.

(b) *Spatial specificity: high-resolution imaging*

In fMRI studies, there are two reasons for concern regarding spatial specificity: one is the sensitivity to different size blood vessels and the presence of macrovascular contribution and the second is the spatial specificity of the physiological and metabolic events that ultimately yield the functional images.

The issue of spatial specificity and resolution of fMRI can be addressed using specific experiments targeted at mapping functionally distinct structures with well-defined organization and topography in the human brain. Early experiments introducing the fMRI methodology employed such a strategy and examined the hemispheric lateralization in brain function (Bandettini *et al.* 1992;

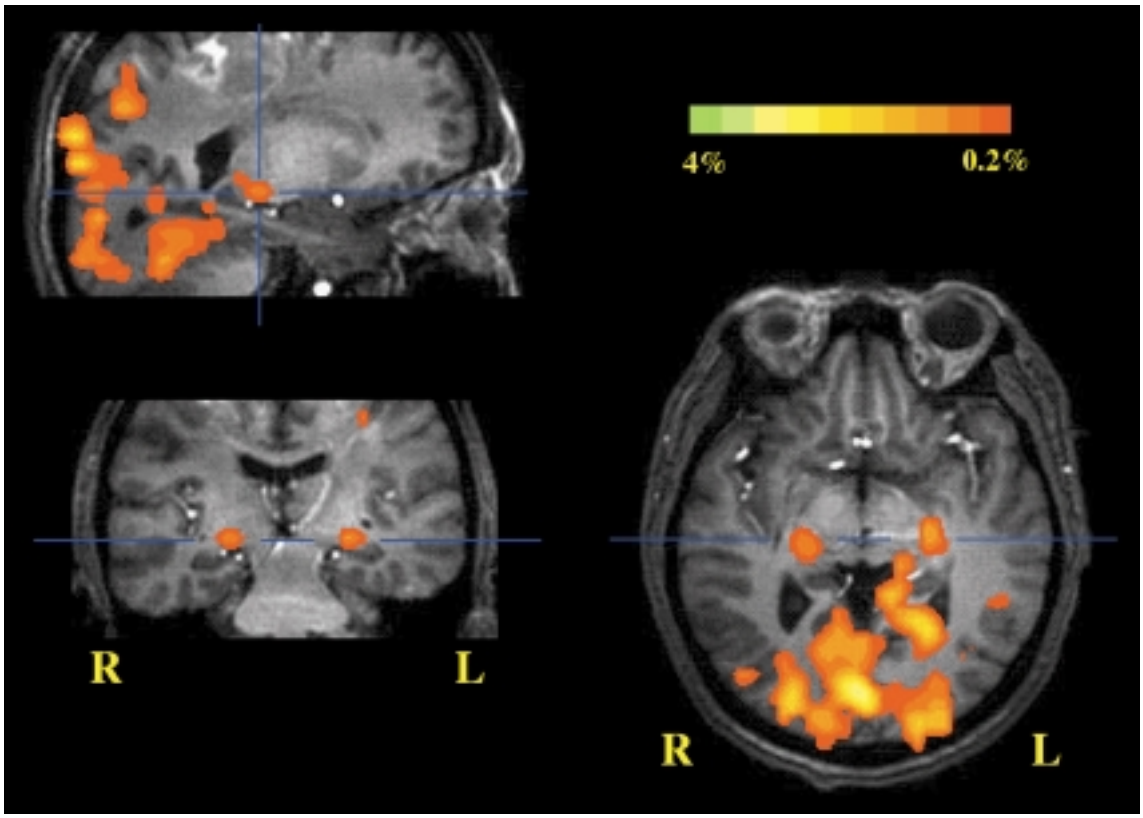

Figure 8. Detection of LGN activation together with activation in the visual areas of the occipito-temporal cortex during visual stimulation by a light-emitting diode (LED) goggle. Three orthogonal slices are illustrated. A multislice fMRI data set covering the whole brain was assembled to generate 3D functional and anatomical images. The LGN appears bilaterally in the coronal and axial slices (lower row) at the level of the blue line and is shown for one of the two hemispheres in the sagittal image where the two blue lines cross. The blue line(s) in each image also identify the relative position of the other orthogonal slices. From Chen *et al*. (1998).

Kwong *et al*. 1992; Ogawa *et al*. 1992; Ellermann *et al*. 1994). However, detection of functional specialization with respect to hemispheric laterality only reveals the existence of a very coarse level of spatial specificity in the spatial domain which can be characterized as several centimetres. On a much finer spatial scale, e.g. millimetre and submillimetre domains, it is possible to examine activation of small subcortical nuclei and even smaller level neuronal functional organizations such as the ocular dominance columns (ODCs).

The thalamus provides an excellent case for evaluating the question of whether structures which are only a few millimetres in size can be accurately mapped by fMRI methodology and resolved from each other. The thalamus contains several distinct, anatomically well-defined nuclei. These nuclei serve as relay points for a remarkably large number of pathways. For example, the retinal output projects mainly to the lateral geniculate nucleus (LGN) and, to a lesser extent, the pulvinar, two distinct and distinguishable structures within the thalamus which must be activated during visual stimulation.

The LGN is a small, subcentimetre nucleus located posteriorly and ventrally within the thalamus. The LGN is a primary target of retinal afferents and, in turn, it projects to the primary visual cortex (Hubel & Wiesel 1968, 1972, 1977; Hubel *et al*. 1974; Rakic 1976). A very strong back projection from V1 to the LGN is also present. We recently examined (Chen *et al*. 1998) whether LGN activation in the human brain during photic stimulation can be robustly detected and distinguished from adjacent structures, such as the pulvinar, which are expected to be engaged in visual stimulation using fMRI at high magnetic fields (4 T). In this trial, the multislice capability of fMRI to generate a 3D functional map of the whole brain was used so as to resolve the LGN from adjacent relevant structures. Figure 8 illustrates images of V1 and bilateral functional activation of the LGN in one participant in three different planes; these planes were extracted from the 3D data set by 'reslicing'. In the axial image, the LGN in the two hemispheres are easily identified by their position relative to the optic tract; posteriorly from the optic chiasm, the optic tract runs adjacent to the cerebral peduncle in the mid-brain and directly joins the LGN. In the axial image illustrated in figure 8, the optic tract is seen clearly in both hemispheres near the optic chiasm, anterior to the mid-brain; proceeding posteriorly from the optic chiasm, it appears to merge with the mid-brain and is no longer visualized with clarity as it runs along the cerebral peduncle. Following this curved tract should lead directly to the LGN, which is where the activated loci identified as the LGN are situated. In the coronal and parasagittal views, this activated area appears superior to the hippocampal formation as expected for the LGN (Chen *et al*. 1998; see also the brain anatomy identified in Duvernoy (1991) and Nolte (1993)).

Figure 9 illustrates three anatomical images in the top row, two (labelled as (*c*) and (*e*)) taken from a brain atlas (Duvernoy 1991) and the third (labelled as (*a*)) from a

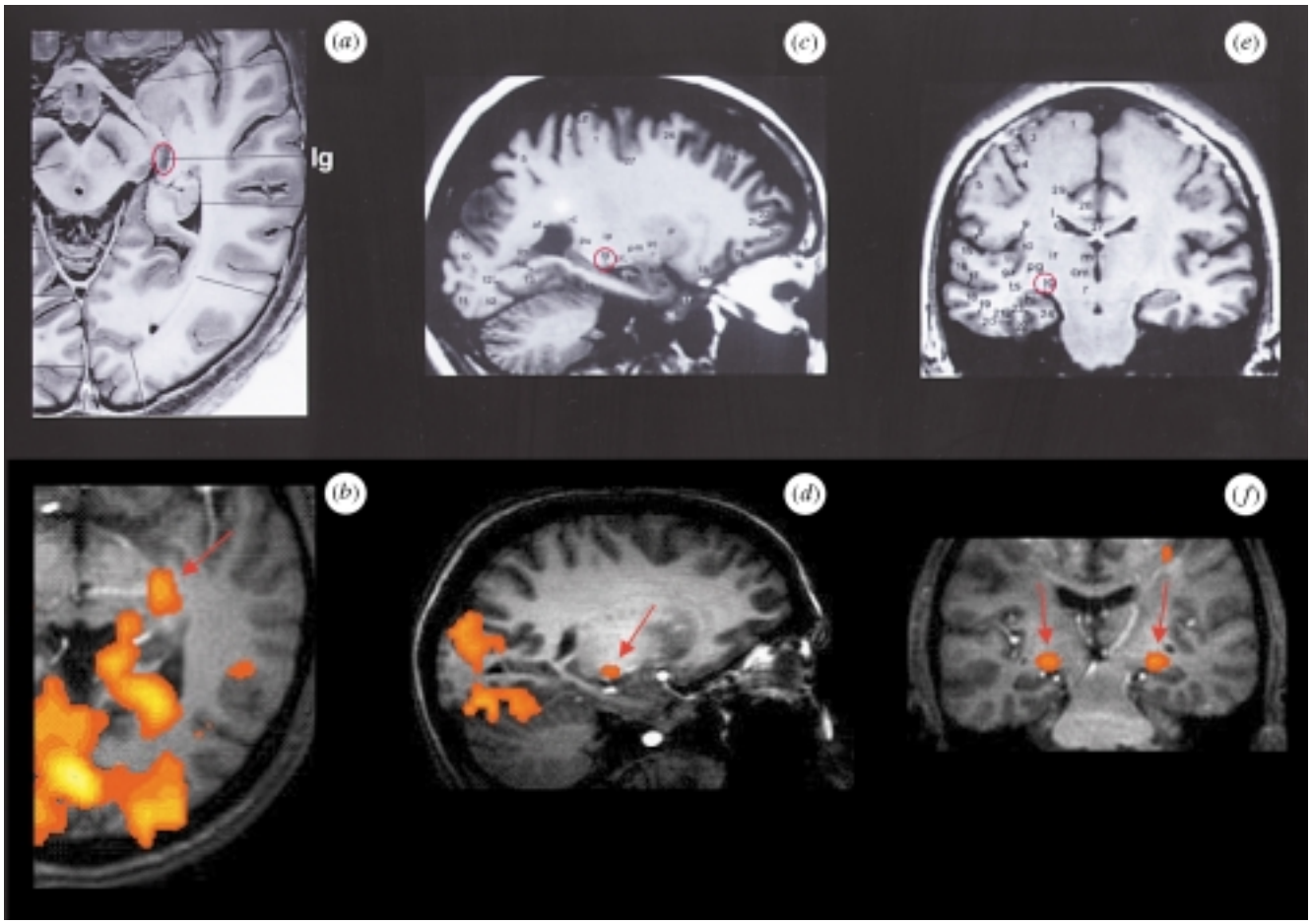

Figure 9. Comparison of anatomical identification of the LGN and the functional activity detected in this study in two different subjects and in three orthogonal planes. The top row illustrates three anatomical images ((*a*) is from Nolte (1993, p. 291) and (*c*) and (*e*) are from Duvernoy (1991, pp. 152 and 270)). The LGN is identified as lg and is circled in red. The lower row illustrates three fMRI images in three different planes from two different subjects. (*b*, *f*) fMRI maps (axial and coronal orientations) created from a single experiment in one individual subject (the same subject as the one illustrated in figure 8). (*d*) The composite fMRI map (sagittal orientation) created from three experiments in another individual subject. The arrows depict the sites of LGN activation. The image planes are virtually identical for our images and the corresponding images taken from the reference books.

textbook on the brain (Nolte 1993); these images display three orthogonal slices that contain the LGN and identify this structure (labeled as lg and circled in red) as well as others. Figure 9 also illustrates three fMRI images in three different planes from two different subjects ((*b*) and (*f*) are from one subject (the same subject as the one illustrated in figure 8) and (*d*) is from another subject). The image planes are virtually identical for the fMRI images and the corresponding images taken from the reference books. The agreement of the anatomical location of the activation identified as the LGN with the anatomical identification of the LGN is perfect. Also note the excellent correspondence of the sagittal view of LGN activation displayed in figure 8 with the sagittal anatomical slice taken from the brain atlas (figure 9*c*).

Primate studies have suggested that the pulvinar nucleus is an integral part of the extrageniculate visual pathway (Ogren & Hendrickson 1976; Rezak & Benevento 1979; Bender 1981, 1982; Robinson & Petersen 1992). The pulvinar nucleus, in particular the inferior and adjacent lateral parts, are located in close proximity to the LGN in the thalamus; detection of pulvinar activation and distinguishing it from the activation in the adjacent LGN requires specificity of fMRI at the few millimetre spatial scale. In addition, fMRI data acquisition must be performed appropriately to provide means of distinguishing these two structures. Single-slice image acquisition, for example, would make it difficult to locate the LGN position anatomically and distinguish it unequivocally from nearby areas of the thalamus. An example of where this difficulty was encountered is the earlier work aimed at examining the detectability of the LGN activation by fMRI. In this previous fMRI study, the LGN activation during visual stimulation was reported to be observable by correlating the temporal responses of signals from the primary visual cortex with those in the LGN regions (Kleinschmidt *et al.* 1994); however, the region where the activity was reported is likely to be pulvinar. A later study at 1.5 T covering several slices reported detecting the LGN successfully and showed that intersubject averaging can be used for the detection of this thalamic nucleus (Buchel *et al.* 1997). In the 3D studies of Chen *et al.* (1998) both LGN and pulvinar activity was detected and resolved; this is illustrated in figures 8 and 10 in three orthogonal slices 'resliced' out of the 3D functional and anatomical images. The sagittal

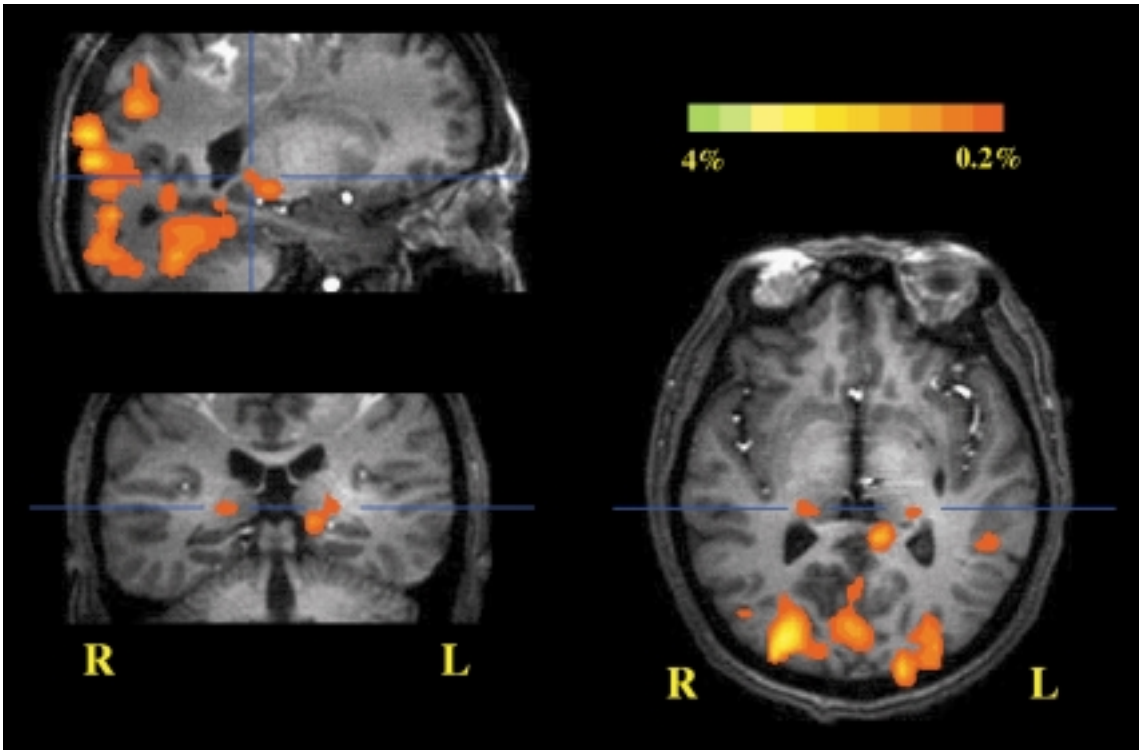

Figure 10. Detection of pulvinar activation together with activation in the visual areas of the occipito-temporal cortex during visual stimulation by an LED goggle. From the same data set as figure 8. The sagittal slice is the same. From Chen *et al*. (1998).

slices in figures 8 and 10 show both LGN and pulvinar activation which appear contiguous but resolved in this plane. The axial and coronal slices taken at the positions indicated by the blue lines demonstrate the two different nuclei clearly, the LGN in figure 8 and the pulvinar in figure 10.

The LGN is also functionally and spatially segregated and compartmentalized. Each of six LGN layers receives inputs from the specific visual field via the retina and then retinotopically projects to V1 (Zeki 1993). Recently, we conducted such a study using a checkerboard visual stimuli with a different visual field (Chen *et al*. 1999) examining the use of high-resolution fMRI for mapping the retinotopic organizations in the small LGN. In this study, one of the visual stimulation paradigms used was either upper- or lower-hemifield stimulation against a dark control period. This is expected to activate the LGN bilaterally. However, the most striking question is whether the retinotopic relationship reflecting the upper versus lower visual field can be detected and distinguished within the LGN. This is illustrated as composite maps for four individual subjects in figure 11. In this figure, yellow and green pixels represent the LGN activation corresponding exclusively to the lower and upper visual field stimulations, respectively; the red pixels represent the overlap. The LGN activation induced by upper visual field stimulation (i.e. green and red pixels) was more inferior in location (closer to the hippocampal formation) compared to that induced by lower visual field stimulation (i.e. yellow and red pixels). This relationship is consistent with the non-human primate visual system which has been extensively studied using microelectrode recording (Malpeli & Baker 1975) and selective lesions (Schiller *et al*. 1990*a*,*b*). Our results also illustrate that the LGN in humans behaves similarly to V1 (Sereno *et al*. 1995). However, the upper and lower visual field representations in V1 are anatomically separated by the calcarine fissure and are distinguishable without overlap. In contrast, they are continuous in LGN layers. This contributes to the partial overlap of LGN activation between the upper and lower visual fields (figure 11).

From the LGN, geniculostriate projections to the primary visual cortex (V1) continue to carry left- or right-eye input separately and terminate in layer IVC of V1 where they are arranged in a system of roughly parallel alternating stripes, i.e. the ODCs. In non-human primates and other vertebrates, the organization of these columns has been studied by histological stains, autoradiography and microelectrode recordings (e.g. Kennedy *et al*. 1976; Hubel & Wiesel 1977; Le Vay *et al*. 1985) and by optical imaging of intrinsic signals (Grinvald *et al*. 1986, 1991; Frostig *et al*. 1990; Ts'o *et al*. 1990; Malonek & Grinvald 1996). In humans, the ODCs have been demonstrated post mortem in striate cortex by histochemical staining for cytochrome oxidase (Horton & Hedley-White 1984; Horton *et al*. 1990), but a non-invasive technique for examining human striate cortex organization on the scale of cortical functional subunits has not been available.

The haemodynamic response mechanism that allows visualization of orientation columns and ODCs in awake monkeys by optical imaging of intrinsic signals demonstrates that corticovascular responses to visual stimuli can be localized to the columnar level in several mammalian species. In particular, the optical data demonstrate that, while the CBF response may not be specific at the ODC level (Malonek & Grinvald 1996), a deoxyhaemoglobin difference across the active and inactive columns is

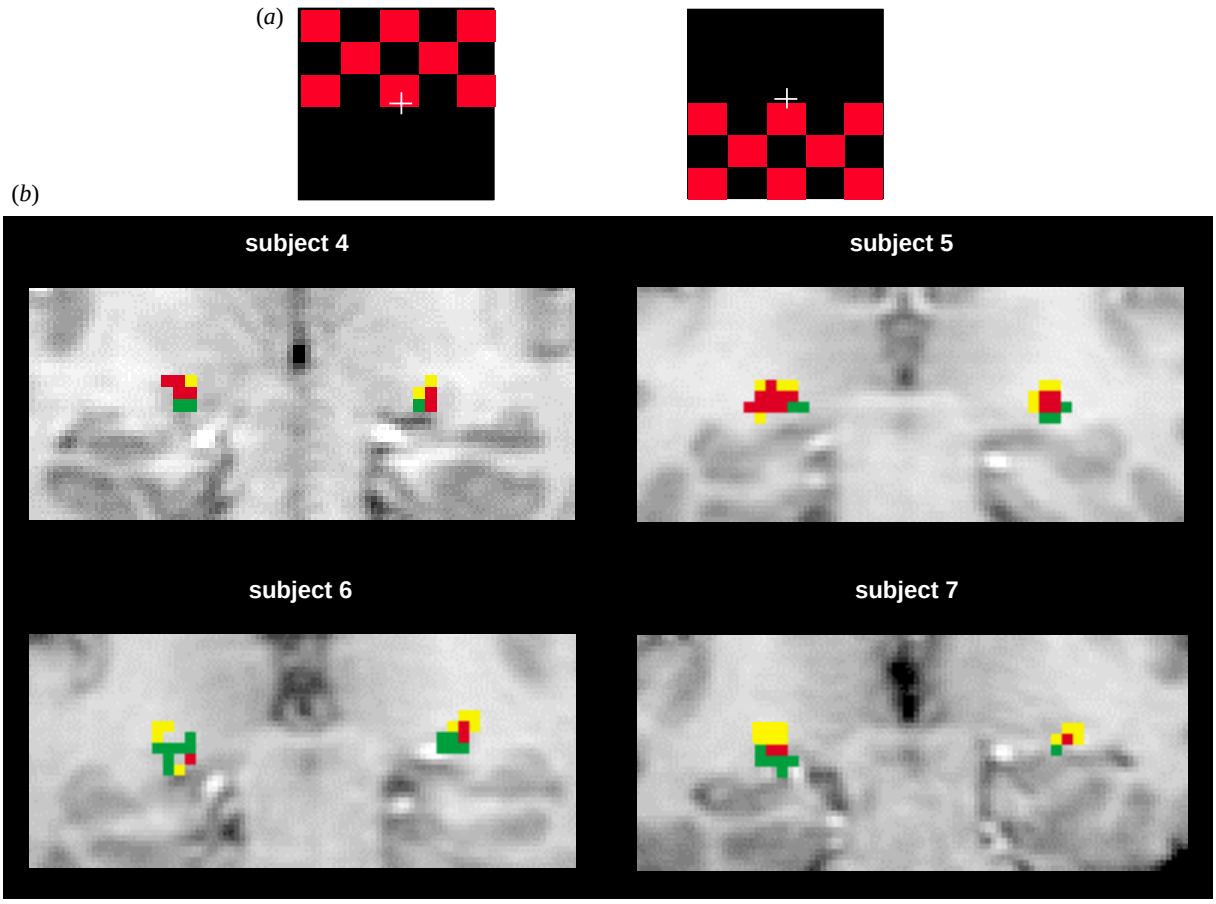

Figure 11. (*a*) High-resolution fMRI mapping of LGN activation during the upper-field and lower-field red–black checkerboard visual stimulations. Images are in the coronal orientation. (*b*) The activation in colour represents composite fMRI maps obtained by combining the activation maps generated by (i) upper visual field stimulation versus a dark control period and (ii) lower visual field stimulation versus a dark control period. The red pixels represent the overlap between these two activation maps. Yellow and green identify pixels activated only by lower- and upper-field stimulations, respectively (adapted from Chen *et al.* (1999)).

generated presumably because of the enhanced $CMRO_2$ in the active but not in the inactive column. This deoxyhaemoglobin signal should in principle be detectable by BOLD-based fMRI provided the technique has sufficient specificity as well as sensitivity (signal-to-noise ratio) to achieve the required high spatial resolution. For example, if large vessel contributions dominate the BOLD contrast observed, adequate specificity will not be present to detect ODCs.

For fMRI studies using clinically available hardware, *ca.* 3 mm in-plane resolution and *ca.* 5 mm slices are typical because of the limited signal-to-noise ratio available without extensive data averaging. Using the same high-resolution fMRI pulse sequence with imaging hardware and parameters optimized at three different field strengths, we have found that the signal-to-noise ratio at 4 T is at least four times higher than at the much more commonly available 1.5 T field strength (Gati *et al.* 1995, 1997). This increase is sufficiently large to attempt imaging of ODCs in human V1, which are approximately 0.8–1 mm on a side for a column and 5–10 mm long in humans (Horton & Hedley-White 1984; Horton *et al.* 1990). Using a simple visual paradigm in combination with an optimized radio-frequency coil, head restraints, subvoxel image registration and the enhanced signal-to-noise ratio provided by 4 T, it has been possible to demonstrate adjacent image pixels in human V1 that respond primarily to left or right eye photic input (Menon *et al.* 1996, 1997).

Figure 12*a* demonstrates a magnified picture of a cortical ribbon along a sulcus in the primary visual cortex. The image plane is along the calcarine fissure so that columns should appear as *ca.* 1 mm × 1 mm rectangles separated by *ca.* 1 mm in the cortical grey matter. The colour map here represents pixels that had higher signal intensity during left versus right eye monocular photic stimulation. The dimensions of the 'activated' pixels are approximately 1 mm × 1 mm or slightly smaller. These pixels are also located not only in the grey matter but in the middle of the cortical ribbon as expected. Furthermore, they have been shown to be reproducible (Menon *et al.* 1996, 1997). The paradigm in this study was to first use a binocular stimulation and then to use alternating left–right monocular stimulation. However, the data were analysed by looking for statistically significant differences in pixel intensities only for the monocular stimulation period, ignoring the binocular stimulation completely. The pixels identified as 'activated' during either the

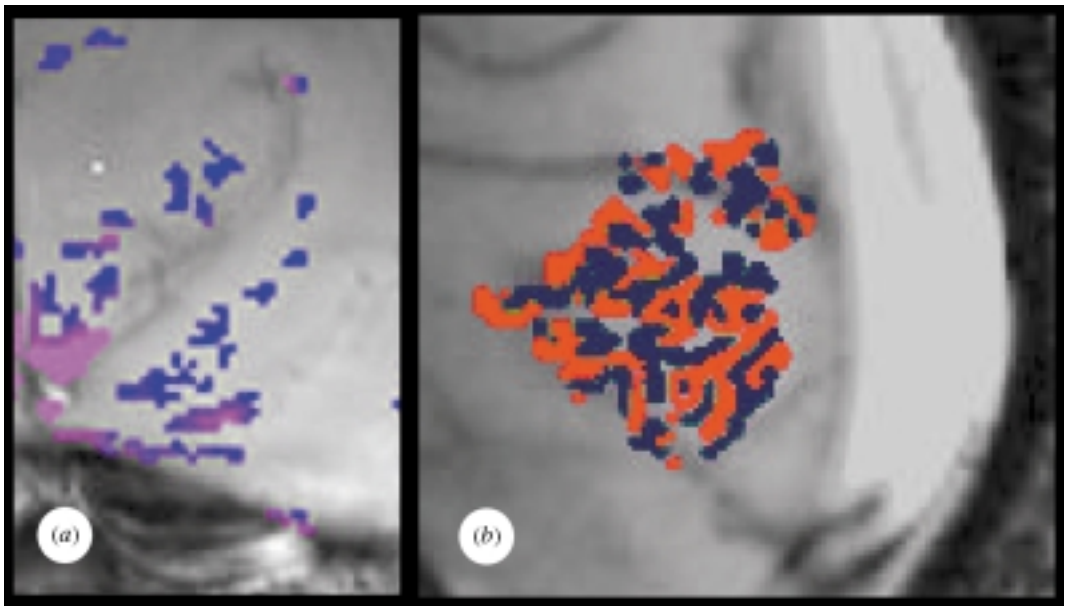

Figure 12. Detection of human ODCs during alternating monocular stimulation at 4 T. (*a*) A study obtained on a plane parallel to the calcarine fissure that intersects the ODCs perpendicular to their long axis. In this view, the ODCs should appear approximately as squares of 1 mm × 1 mm cross-section, separated by *ca*. 1 mm. We see a curving sulcus lined by the ODCs (from Menon *et al*. 1997). (*b*) A more recent study at 4 T by Menon *et al*. (1999) showing a sagittal plane adjacent to the interhemispheric fissure so that the ODCs are visualized as they appear on the cortical surface. The blue and red colours illustrate the columns associated with the two different eyes (Goodyear & Menon 1999).

left- or right-eye monocular stimulation also showed activation for the binocular period, as they should if they indeed represent ODCs as opposed to random statistical correlations.

Figure 12*b* demonstrates ODCs in the human brain from a more recent study at 4 T by Goodyear & Menon (1999). These images were obtained in the sagittal plane adjacent to the interhemispheric fissure so that the ODCs are visualized as they appear on the cortical surface in this region of the visual cortex. The blue and red colours illustrate the columns associated with the two different eyes. The columns are now seen not in cross-section but along their long axis.

These data, to our knowledge, demonstrate for the first time that mapping of functional subunits in humans is possible in a non-invasive manner. The fMRI time-courses show that the haemodynamic response at the 'hyperoxygenation phase' can be used at 4 T as a direct indicator of neuronal activity in cortical columns. This opens up the possibility of mapping specialized populations of neurons in humans that are not accessible to electrophysiological or other methods of invasive mapping. However, they do not yet resolve the issue of whether CBF increase coupled to increased neuronal activity and, consequently, BOLD response is spatially specific and selective at the column level. The column images illustrated in figure 12 were obtained using alternating monocular stimulation. Therefore, columns would have been detectable as long as there was a difference in the deoxyhaemoglobin content of the inactive versus active columns and, hence, a difference in the BOLD effect, even if the deoxyhaemoglobin content and consequently the BOLD effect changed for both active and inactive columns. Malonek & Grinvald (1996) suggested that the CBF response is non-specific at the level of orientation columns and leads to oxy- and deoxyhaemoglobin changes in both columns during activation of only one column; however, they also showed that there is a difference in the deoxyhaemoglobin content of the active versus the inactive columns, presumably because the oxygen consumption rate increased more in the active column. This would then imply the presence of a BOLD response in both columns when only one is active but with a difference in the magnitude of the BOLD effect for the active versus the inactive column.

The results summarized above demonstrate that, despite the presence of several potential problems, fMRI at 4 T has the specificity and sensitivity to map organizations at the millimetre or a slightly smaller scale with the use of the appropriate paradigms. This is unprecedented in human brain studies. We must emphasize the high-field aspect of all of the aforementioned high-resolution studies; to date ODCs have not been reported at the lower field strength.

(c) *Early negative BOLD response*

Optical measurements in animal experiments have demonstrated that the onset of task-related activation first results in signal changes interpreted as an increase in deoxyhaemoglobin content, presumably due to increased $CMRO_2$ while CBF changes lag behind (Frostig *et al.* 1990; Malonek & Grinvald 1996). This deoxyhaemoglobin increase peaks at *ca*. 3 s after task onset and is subsequently reversed, ultimately resulting in a relatively large decrease in overall deoxyhaemoglobin content. If $CMRO_2$ is elevated due to energy requirements of increased neuronal transmission, O_2 extraction and, consequently, the deoxyhaemoglobin level will also be elevated provided the blood flow remains constant. In contrast, a CBF increase alone without any alterations in

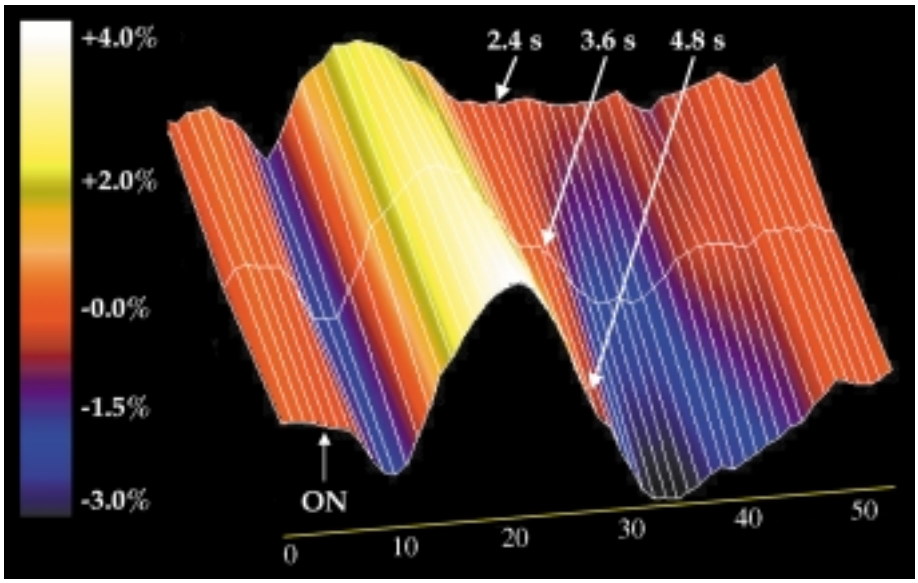

Figure 13. Signal intensity time-course for activated areas in the primary visual cortex for three different periods of brief visual stimulation of 2.4, 3.6 and 4.8 s. Initially the signal decreases, ending up in a valley, which is the early negative response or 'dip'; subsequently, the signal increases leading to a peak which corresponds to the positive BOLD effect employed in functional images. This positive BOLD effect is much larger in magnitude than the early negative BOLD effect. Note that the post-stimulation undershoot comes in prominently only as the visual stimulation gets longer in duration. From Hu *et al*. (1997).

$CMRO_2$ will only cause a decrease in deoxyhaemoglobin; if there is a difference in the metabolic and haemodynamic response times of these two processes, with the latter lagging behind, the time dependence of deoxyhaemoglobin content in the 'activated' region will be biphasic. Alternatively, there may be a component of blood volume increase which is rapid and precedes the elevation in blood flow in time; such a volume increase would result in elevated oxy- and deoxyhaemoglobin contents while a subsequent rush of oxygenated blood due to enhanced blood flow would then decrease the deoxyhaemoglobin level provided oxygen use does not increase commensurately with CBF.

Malonek & Grinvald (1996) argued that the early response is spatially more specific and better defined the columnar structure examined in the cat visual cortex in that study. In contrast, they suggested that CBF increase is not as specific, flooding not only the active but also inactive columns and surpassing in spatial extent the actual area of activation by several millimetres. These claims suggest that the BOLD effect associated with the hyperoxygenated, high flow phase during increased neuronal activity will also be spatially non-specific at the several millimetre scale, reflecting the spatial distribution of the CBF response. The question then arises as to whether the early response associated with increased deoxyhaemoglobin can also be detected as a negative signal change in BOLD-weighted MRI and whether this response can be used as a means of obtaining functional images with the MRI approach.

An early negative response was first reported by Ernst & Hennig (1994) using a spectroscopy method monitoring signal from a relatively large voxel but with high temporal resolution. Subsequently, imaging studies first involving multiple subject averaging (Menon *et al*. 1995) and later in single subjects documented the presence of a small but detectable early negative signal change, a 'dip', from our group (Tuong & Hu 1996; Hu *et al*. 1997) and others (McIntosh *et al*. 1996; Moore *et al*. 1997; Twieg *et al*. 1997) at high magnetic fields. Figure 13 illustrates the time dependence of BOLD contrast fMRI signal changes observed in the human visual cortex during and subsequent to a brief visual stimulation that lasted 2.4, 3.6 and 4.8 s (Hu *et al*. 1997). In this study, T_2^*-weighted, gradient-recalled echo-planar images were acquired rapidly covering only a few slices in the visual cortex, thus sacrificing spatial extent of coverage and spatial resolution in favour of time resolution. Furthermore, the brief stimuli were repeated several times (four to ten) and images were collected in synchrony with the stimulus presentation so that they could be averaged. The data revealed that, during and following the brief visual stimulation period, the BOLD-based fMRI signal initially decreased and this decrease was reversed at *ca*. 3 s, subsequently resulting in a large signal intensity increase (figure 13). For the longer stimulation period, a signal intensity decrease below baseline was also seen towards the end of the time-course; this 'late-phase', post-stimulation decrease has been observed before, even in the very first fMRI papers and may reflect a difference in the post-task temporal responses of blood volume (Mandeville *et al*. 1998*b*) and/or $CMRO_2$ (Frahm *et al*. 1996) returning to basal levels much slower than blood flow.

Figure 14 displays visual stimulation activation maps in the sagittal plane constructed from these data, with the early negative signal changes colour coded in blue–purple colours and the later positive response coded in red–yellow colours. Examining the images constructed from data during the early (negative) versus the late (positive) response, we see that the early response is restricted to the anatomically well-defined visual area V1 along the calcarine fissure, while the later 'positive' BOLD image displays apparent 'activation' in areas distant from this region; in this study, these distant areas represent

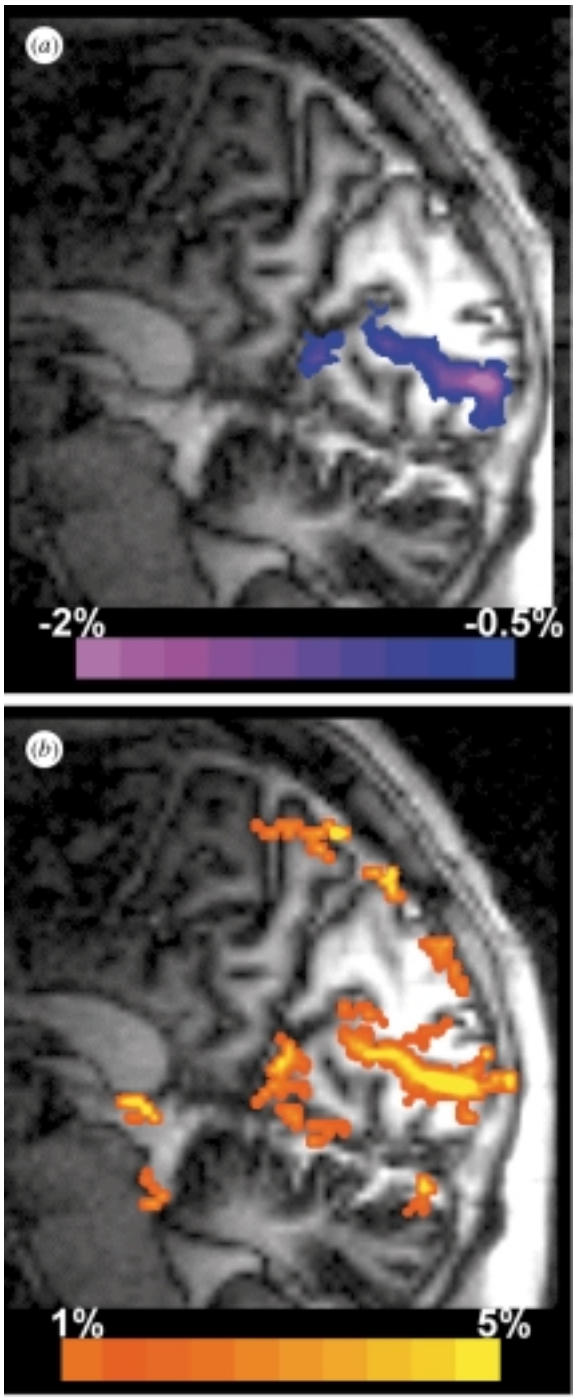

Figure 14. Functional images of visual stimulation constructed from (*a*) the early negative response (colour coded in blue) and (*b*) the peak of the subsequent positive response (colour coded in yellow–red). From Hu *et al.* (1997).

'artefacts' associated with the MRI methodology, namely the macrovascular inflow effect. The macrovascular inflow effect was not suppressed in these images because they were rapidly acquired and were obtained using a surface coil both for signal detection and excitation; thus, it was practically impossible to achieve the condition of 'full relaxation' in between images that would have eliminated these artefacts without significantly sacrificing signal-to-noise ratio. The macrovascular inflow effect does not appear in the early images because it is not there due to the slower haemodynamic response time. If the

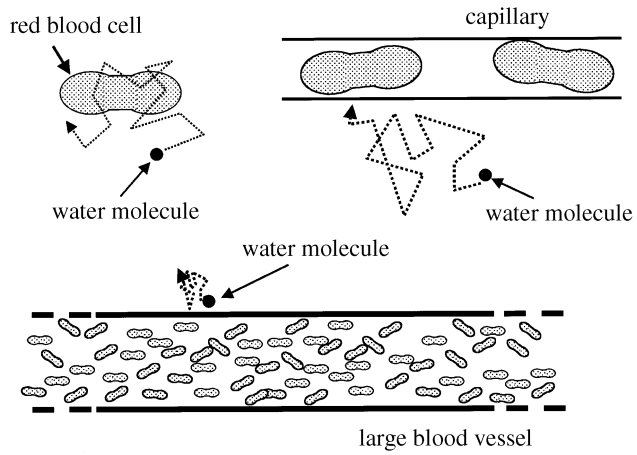

Figure 15. Dynamic and static averaging regimes based on diffusion distances relative to the size of the compartment, which differs in magnetic susceptibility compared to the surrounding space. The magnetic field gradients are most prominent in the vicinity of the compartments with different susceptibility, i.e. red blood cells, capillaries and large blood vessels and diminish outside of the compartment over distances that approximate the compartment dimensions. In the case of the red blood cells and capillaries, water diffusion in times relevant to the BOLD fMRI experiment (e.g. 25–70 ms) averages the magnetic field gradients. In the case of the large blood vessels, diffusion distances are not large compared to the vessel radius and, hence, do not lead to dynamic averaging.

macrovascular effects are ignored and the functional maps around the calcarine fissure are compared, we see that they are similar for the early negative and the later positive BOLD images. This observation has implications with respect to the spatial specificity of the functional maps generated by fMRI. It suggests that, provided the macrovascular 'inflow' artefacts are eliminated, at the resolution of this study (*ca.* 3–4 mm isotropic) the spatial specificity of the early negative BOLD-based maps and the later ΔCBF-dominated, positive BOLD images are very similar. However, this study does not yet answer the question of spatial specificity raised by Malonek & Grinvald (1996) because the fMRI study was not conducted at a sufficiently high spatial resolution. It is likely that higher magnetic fields will be necessary to achieve greater spatial resolution with this early response because it is a very weak effect. The fact that it is detectable by BOLD-based fMRI, however, is significant, both from a mechanistic point of view and for future developments in fMRI.

(d) *Experimental studies of vessel sizes and intra- versus extravascular BOLD effects in fMRI*

Early in the history of fMRI, it was experimentally demonstrated that the BOLD effect in human brain functional maps contains contributions from macroscopic venous blood vessels (i.e. vessels of *ca.* 0.5 mm or larger that can be visualized in MRI images) as well as from regions where no such macroscopic vessels were identified (Menon *et al.* 1993). This has profound implications for the effective spatial specificity and spatial resolution that can be achieved with fMRI since large blood vessels do not exist at high density in the brain, as do the capillaries.

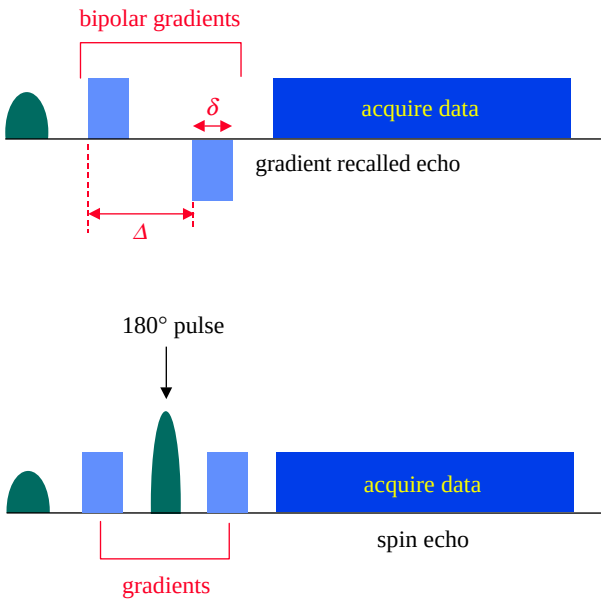

Figure 16. Pulse sequence diagrams illustrating the time sequence of the RF pulse(s) for signal excitation, gradient pulses (known as 'bipolar' or 'diffusion weighting' gradients) for motion sensitization and data acquisition in a gradient and spin-echo sequence. Gradients for spatial encoding for image generation are not shown.

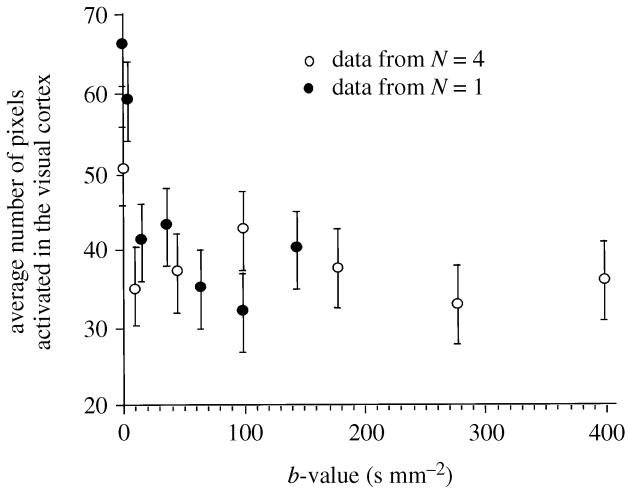

Figure 17. Number of activated pixels in the human visual cortex during visual stimulation at 4 T before and during application of bipolar gradients with increasing *b*-value. The sequence was a spin-echo sequence yielding T_2-weighted BOLD images. The residual signal intensity that persists at high *b*-values can come only from the microvasculature. From Menon *et al.* (1994).

Therefore, functional maps based on macrovasculature can be significantly distant from the actual site of increased neuronal activity and, thus, misleading if high-resolution mapping at the millimetre or a smaller scale is desired. The effect of the blood vessel size on BOLD will depend on magnetic field strength and the relative contributions of intra- versus extravascular effects.

In the blood, haemoglobin is compartmentalized within red blood cells. Thus, when the deoxy form is present, there are field gradients around the red cells. However, because the dimensions are very small compared to diffusion distances, the effect is dynamically averaged by diffusive motion of the water molecules (figure 15) and only becomes a T_2 effect, as opposed to a T_2^* effect. The dynamic averaging in this case also involves exchange across the red blood cell membrane, which is highly permeable to water. Thus, in the presence of deoxyhaemoglobin-containing red blood cells, the T_2 of blood decreases. This effect was noted by Thulborn *et al.* (1982, 1992) and was shown to increase quadratically with field strength as expected. Therefore, the T_2 of blood itself will change when the deoxyhaemoglobin content is altered by elevated neuronal activity and this will lead to a signal change in a BOLD-weighted image. This intravascular BOLD effect will be present wherever the deoxyhaemoglobin content has changed, thus potentially both in large and small blood vessels.

The extravascular BOLD effect is associated with the magnetic field gradients generated outside the luminal boundaries of the blood vessels due to the deoxyhaemoglobin-induced magnetic susceptibility difference between the blood vessel and the surrounding diamagnetic tissue. When these blood vessels are small (for 4 T *ca.* 5 μm given the typical deoxygenation state of the capillary or venous blood), these magnetic field gradients are dynamically averaged and result in a T_2 effect, just like the intravascular BOLD effect. However, when the blood vessel dimensions are large, dynamic averaging is not possible. Instead, there will be 'local' or 'partial' dynamic averaging over a subsection of the volume spanned by the magnetic field gradients generated by the blood vessel (figure 15). However, there will be signal loss from the voxel due to static averaging if refocusing pulses are not used. A water molecule at a given point in space relative to the blood vessel will see a 'locally' time-averaged precession frequency about the static magnetic field, $\bar{\omega}_B$, which will vary with proximity to the large blood vessel. Because $\bar{\omega}_B$ varies across the voxel, the signal for the entire voxel will be 'dephased' and lost during the delay employed in BOLD weighting after signal excitation and prior to signal acquisition (echo time t_e). This signal loss occurs from 'static averaging'. In this regime, if the variation $\bar{\omega}_B$ over the voxel is relatively large, signal decay can be approximated with a single exponential time constant T_2^*. In a spin-echo experiment, this static averaging will be eliminated and will not come into play since the dephasing will be reversed after the application of a 180° pulse prior to signal acquisition.

The origin of the signal intensity changes that are detected in T_2- versus T_2^*-based BOLD fMRI images differ significantly. The T_2^*-based BOLD signal can arise from both intravascular (blood) and extravascular effects originating from large and small blood vessels. The relative contributions of these effects will depend on the magnetic field strength. In a T_2-based BOLD fMRI map, the signal changes come from (i) intravascular, blood T_2 changes and, hence, from both large and small blood vessels, and (ii) the extravascular effect associated only with microvessels such as capillaries and small venuoles. Thus, the major difference is that the extravascular BOLD effect in a T_2 image can only arise from the microvasculature.

The issue of the extra- versus intravascular BOLD effect has been experimentally examined using bipolar

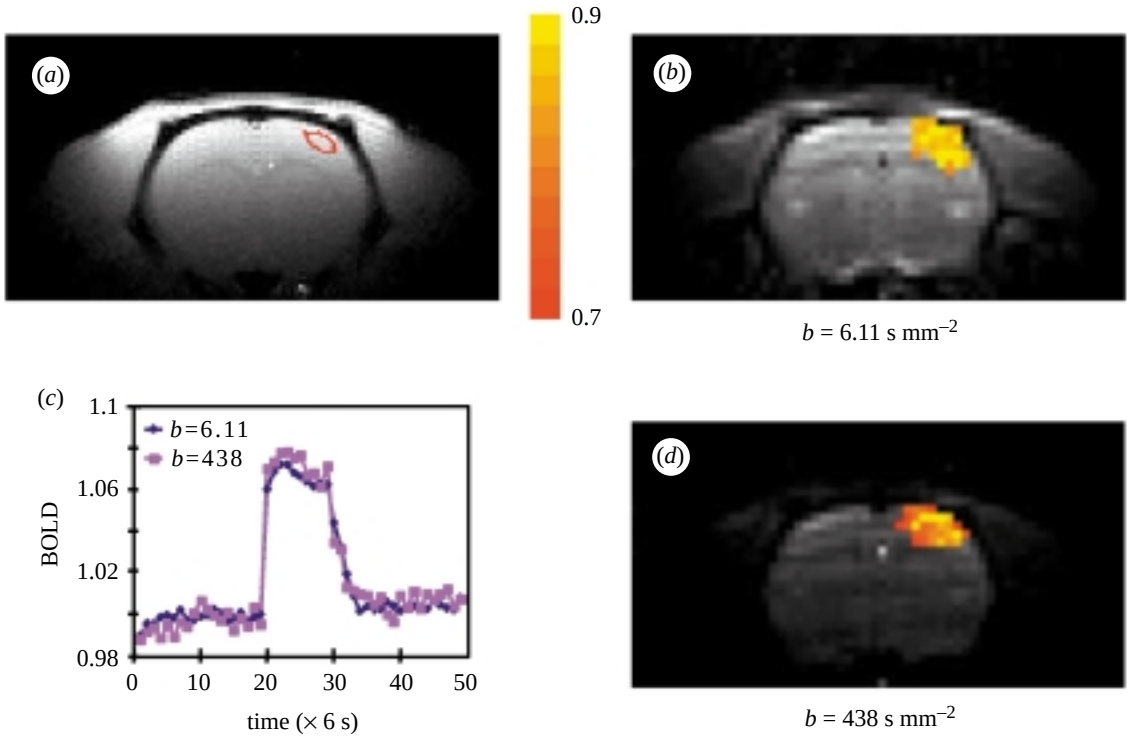

Figure 18. 9.4 T, diffusion-weighted, spin-echo fMRI maps with b-values of (*b*) 6.11 and (*d*) 438 s mm^{-2} overlaid on one of the original, consecutively acquired EPI images (BOLD and diffusion weighted) collected during the functional imaging study. Coronal single-slice, single-shot, spin-echo EPI images of rat brain were acquired with a matrix size of 64 × 32, a field of view of 3.0 cm × 1.5 cm, a slice thickness of 2 mm and $t_e = 30$ ms. Somatosensory stimulation was used. The colour bar indicates a maximum cross-correlation value of 0.7–0.9. Signal intensity (shown in the background) was significantly reduced by bipolar gradients, as expected due to diffusion. Localized activation is observed at the somatosensory cortex in the contralateral side of a stimulated forepaw. Foci of activation site (colour) agree very well in both fMRI maps. A Turbo FLASH image with a region of interest (ROI) is shown in (*a*) and time-courses of diffusion-weighted images within the ROI are shown in (*b*). If the macrovascular contribution was significant, relative BOLD signal changes would decrease when a higher b-value is used. However, the relative signal changes remained the same in both images, suggesting that extravascular and microvascular components predominantly contribute to spin-echo BOLD at 9.4 T. From Lee *et al.* (1999).

gradients. In an fMRI experiment, images are collected subsequent to signal excitation and echo formation, either by a gradient reversal or application of a refocusing radio frequency (RF) pulse, as previously discussed. During the delay after excitation and before echo formation, it is possible to apply a pair of gradient pulses (i.e. to turn on and off 'inhomogeneous' magnetic fields that vary with space) with opposing or same polarity depending on whether the experiment is a gradient-recalled echo or a spin-echo experiment, respectively (figure 16). When the water molecules are static in time, then such gradient pulses will ideally have no effect on the image. In the presence of diffusion, such pulses will lead to signal loss since the spatially dependent dephasing during the first part of the gradient pulses will not be redone. This pulsed gradient pair for diffusion measurements was introduced by Stejskal & Tanner (1965); hence, the use of such gradients to alter the image signal intensity is often referred to as 'diffusion weighting' even though there are additional perturbations that arise from the use of such gradients.

In experiments employing the Stejskal–Tanner gradients, the important parameters are the magnitude and the duration of the gradient pulse and the time separation between them. Frequently, the results are evaluated in terms of a parameter b which is equal to $(\gamma G\delta)^2(\Delta - \delta/3)$, where γ is the gyromagnetic ratio (rad s^{-1} G^{-1}), G is the magnetic field gradient magnitude (G cm^{-1}), δ is the duration of the gradient pulse and Δ is the separation in time of the onset of the two gradient pulses. In simple isotropic diffusion, the MRI signal in the presence of Stejskal–Tanner gradients decays according to $\exp(-bD)$ where D is the diffusion constant. For flowing spins, b does not have such an immediately obvious physical meaning. If there is flow, the spins will acquire a phase that depends on the amplitude of the Stejskal–Tanner gradients, the position of the spin and the velocity of the spins. Within blood vessels, however, flow is not uniform particularly for vessels with a large diameter. Furthermore, the blood vessels may change direction within a voxel and there may be several different blood vessels within the voxel with different flow rates and/or different orientations relative to the gradient directions. Since the blood signal detected from the voxel will be a sum of all of these, the net result can be signal cancellation due to dephasing of flowing spins. As a result, these pairs of gradients can suppress flowing spins in blood vessels very effectively.

The Stejskal–Tanner pulsed gradients can be used to distinguish between intra- and extravascular BOLD effects in functional images. Such experiments have been performed at 1.5 and 4 T on humans. The studies at 1.5 T concluded that most of the BOLD-based signal increase

during elevated neuronal activity is eliminated by bipolar gradients, leading to the conclusion that most of the fMRI signal at 1.5 T arises from intravascular effects (Boxerman *et al*. 1995*a*; Song *et al*. 1996). One can even suggest that this intravascular BOLD effect may be associated with only macroscopic blood vessels since it is debatable as to whether the gradient pulses used can suppress intravascular signals from microscopic blood vessels such as capillaries and small venuoles (Henkelman *et al*. 1994). The effect of the Stejskal–Tanner gradients on human brain tissue signal intensity at 4 T is illustrated in figure 17 for a spin-echo sequence (T_2-weighted BOLD effect). When activation studies were performed with such gradients at this field strength, *ca*. 60% of the 'activated' pixels disappeared at small *b*-values but the remaining pixels persisted as the gradient strength was increased to attain very large *b*-values (figure 17). This suggests that, at 4 T, there exist extravascular and/or capillary-level intravascular BOLD effects during activation in addition to a significant intravascular contribution associated with the macrovasculature.

At 9.4 T, the effect of the Stejskal–Tanner gradients becomes even more interesting. In a T_2-weighted fMRI study conducted in the rat brain (forepaw stimulation, symmetric spin-echo with one 180° pulse), we observed that the activation is not altered at all going from very small to very high *b*-values (figure 18). The T_2-based BOLD effect can only come either from blood due to a change in the blood T_2 or from extravascular effects associated with capillaries and comparably sized venuoles. The gradient pair will suppress the blood, except possibly in capillaries and small venuoles. Therefore, one can conclude that, at this ultra high magnetic field, there exists a strong and dominant BOLD effect originating from microscopic vessels. The intravascular effect associated with blood T_2 change is *a priori* not expected to be significant at this field strength due to the fact that the T_2 of venous blood is very short at 9.4 T (*ca*. 5 ms) as previously discussed. Even arterial blood has a short T_2 at this high magnetic field strength (*ca*. 40 ms).

3. CONCLUSION

In conclusion, since its introduction fMRI has rapidly evolved to become the most significant method of investigating human brain function and unique accomplishments have been realized at high magnetic fields. However, it must be realized that high magnetic field MRI instruments are not as optimized and refined machines as clinical scanners. The presence of a high-field magnet does not guarantee superior functional imaging results; instead, advantages that are inherent in the high field for functional mapping can easily be lost due to instrumentation imperfections. Thus, improvements in high-field instrumentation are essential for future expansion of fMRI applications that use high fields. Additional improvements in data collection schemes, motion correction and statistical methods for data analysis, which are areas that are actively pursued, will undoubtedly improve the already impressive capabilities of this methodology, providing neuroscience research with an invaluable tool for examining the unique capabilities of the human brain.

The work reported here from the Center for Magnetic Resonance, University of Minnesota was supported by NIH P41 RR08079, an NIH regional resource grant.

REFERENCES

Bandettini, P. A., Wang, E. C., Hinks, R. S. Rikofsky, R. S. & Hyde, J. S. 1992 Time course EPI of human brain function during task activation *Magn. Reson. Med.* **25**, 390–397.

Belliveau, J. W., Kennedy, D. N., McKinstry, R. C., Buchbinder, B. R., Weisskoff, R. M., Cohen, M. S., Vevea, J. M., Brady, T. J. & Rosen, B. R. 1991 Functional mapping of the human visual cortex by magnetic resonance imaging. *Science* **254**, 716–719.

Bender, D. B. 1981 Retinotopic organization of macaque pulvinar. *J. Neurophysiol.* **46**, 672–693.

Bender, D. B. 1982 Receptive-field properties of neurons in the macaque inferior pulvinar. *J. Neurophysiol.* **48**, 1–17.

Biswal, B., Yetkin, F. Z., Haughton, V. M. & Hyde, J. S. 1995 Functional connectivity in the motor cortex of resting human brain using echo-planar MRI. *Magn. Reson. Med.* **34**, 537–541.

Biswal, B., DeYoe, E. A. & Hyde, J. S. 1996 Reduction of physiological flucuations in fMRI using digital filters. *Magn. Reson. Med.* **35**, 117–123.

Biswal, B., Hudetz, A., Yetkin, F., Haughton, V. M. & Hyde, J. S. 1997 Hypercapnia reversibly suppresses low-frequency fluctuations in the human motor cortex during rest using echo-planar MRI. *J. Cerebr. Blood-Flow Metab.* **17**, 301–308.

Blamire, A. M., Ogawa, S., Uğurbil, K., Rothman, D., McCarthy, G., Ellermann, J. M., Hyder, F., Rattner, Z. & Shulman, R. G. 1992 Dynamic mapping of the human visual cortex by high-speed magnetic resonance imaging. *Proc. Natl Acad. Sci. USA* **89**, 11 069–11 073.

Bloch, F., Hansen, W. W. & Packard, M. 1946 The nuclear induction experiment. *Phys. Rev.* **70**, 474–485.

Boxerman, J. L., Weisskoff, R. M., Hoppel, B. E. & Rosen, B. R. 1993 MR contrast due to microscopically heterogeneous magnetic susceptibilty: cylindrical geometry. In *12th Annual Meeting of the Society of Magnetic Resonance in Medicine.*

Boxerman, J. L., Bandettini, P. A., Kwong, K. K., Baker, J. R., Davis, T. L., Rosen, B. R. & Weisskoff, R. M. 1995*a* The intravascular contribution to fMRI signal change: Monte Carlo modeling and diffusion-weighted studies *in vivo*. *Magn. Reson. Med.* **34**, 4–10.

Boxerman, J. L., Hamberg, L. M., Rosen, B. R. & Weisskoff, R. M. 1995*b* MR contrast due to intravscular magnetic susceptiblity perturbations. *Magn. Reson. Med.* **34**, 555–556.

Broca, P. & Brown-Sequard, C. E. 1855 *Proprietes et fonctions de la moelle epiniere: rapport quelques experiences de M. Brown-Sequard: lu a loa Soceite de biologies le 21 Juillet, Bonaventure et Ducessois.*

Buchel, C., Turner, R. & Friston, K. 1997 Lateral geniculate activations can be detected using intersubject averaging and fMRI. *Magn. Reson. Med.* **38**, 691–694.

Buckner, R. L., Bandettini, P. A., O'Craven, K. M., Savoy, R. L., Petersen, S. E., Raichle, M. E. & Rosen, B. R. 1996 Detection of cortical activation during averaged single trials of a cognitive task using functional magnetic resonance imaging. *Proc. Natl Acad. Sci. USA* **93**, 14 878–14 883.

Buxton, R. B. & Frank, L. R. 1997 A model for the coupling between cerebral blood flow and oxygen metabolism during neural stimulation. *J. Cerebr. Blood-Flow Metab.* **17**, 64–72.

Chen, W., Kato, T., Zhu, X.-H., Strupp, J., Ogawa, S. & Uğurbil, K. 1998 Mapping of lateral geniculate nucleus activation during visual stimulation in human brain using fMRI. *Magn. Reson. Med.* **39**, 89–96. (A published erratum appears in *Magn. Reson. Med* 1998 **39** following p. 505.)

Chen, W., Zhu, X.-H., Thulborn, K. R. & Uğurbil, K. 1999 Retinotopic mapping of the lateral geniculate nucleus in

humans using functional magnetic resonance. *Proc. Natl Acad. Sci. USA.* (In the press.)

Decety, J., Kawashima, R., Gulyas, B. & Roland, P. E. 1992 Preparation for reaching: a PET study of the participating structures in the human brain. *NeuroReport* **3**, 761–764.

Detre, J. A., Leigh, J. S., Williams, D. S. & Koretsky, A. P. 1992 Perfusion imaging. *Magn. Reson. Med.* **23**, 37–45.

Detre, J. A., Zhang, W., Roberts, D. A., Silva, A. C., Williams, D. S., Grandis, D. J., Koretsky, A. P. & Leigh, J. S. 1994 Tissue specific perfusion imaging using arterial spin labeling. *NMR Biomed.* **7**, 75–82.

Duvernoy, H. M. 1991 *The human brain: surface, three-dimensional sectional anatomy and MRI.* Wien, Austria: Springer.

Edelman, R. E., Siewer, B., Darby, D. G., Thangaraj, V., Nobre, A. C., Mesulam, M. M. & Warach, S. 1994 Quantitative mapping of cerebral blood flow and functional localization with echo-planar MR imaging and signal targeting with alternating radio frequency. *Radiology* **192**, 513–520.

Ellermann, J. M., Flament, D., Kim, S.-G., Fu, Q.-G., Merkle, H., Ebner, T. J. & Uğurbil, K. 1994 Spatial patterns of functional activation of the cerebellum investigated using high field (4T) magnetic resonance imaging. *NMR Biomed.* **7**, 63–68.

Ernst, T. & Hennig, J. 1994 Observation of a fast response in functional MR. *Magn. Reson. Med.* **32**, 146–149.

Fox, P. T. & Raichle, M. E. 1986 Focal physiological uncoupling of cerebral blood flow and oxidative metabolism during somatosensory stimulation in human subjects. *Proc. Natl Acad. Sci. USA* **83**, 1140–1144.

Fox, P. T., Raichle, M. E., Mintun, M. A. & Dence, C. 1988 Nonoxidative glucose consumption during focal physiologic neural activity. *Science* **241**, 462–464.

Frahm, J., Kruger, K. D., Merboldt, K. D. & Kleinschmidt, A. 1996 Dynamic uncoupling and recoupling of perfusion and oxidative metabolism during focal brain activation in man. *Magn. Reson. Med.* **35**, 143–148.

Frostig, R. D., Lieke, E. E., Ts'o, D. Y. & Grinvald, A. 1990 Cortical functional architecture and local coupling between neuronal activity and the microcirculation revealed by *in vivo* high-resolution optical imaging of intrinsic signals. *Proc. Natl Acad. Sci. USA* **87**, 6082–6086.

Gati, J. S., Menon, R. S., Uğurbil, K. & Rutt, B. K. 1995 Experimental determination of the BOLD field dependence in tissue and vessels. *Proc. Soc. Magn. Reson.* **3**, 772.

Gati, J. S., Menon, R. S., Uğurbil, K. & Rutt, B. K. 1997 Experimental determination of the BOLD field strength dependence in vessels and tissue. *Magn. Reson. Med.* **38**, 296–302.

Goodyear, B. G. & Menon, R. S. 1999 A neural substrate for eye dominance. *Pers. Commun.* (Submitted.)

Grinvald, A., Lieke, E., Frostig, R. D., Gilbert, C. D. & Wiesel, T. N. 1986 Functional architecture of cortex revealed by optical imaging of intrinsic signals. *Nature* **324**, 361–364.

Grinvald, A., Frostig, R. D., Siegel, R. M. & Bartfeld, E. 1991 High-resolution optical imaging of functional brain architecture in the awake monkey. *Proc. Natl Acad. Sci. USA* **88**, 11 559–11 563.

Henkelman, R. M., Neil, J. J. & Xiang, Q. S. 1994 A quantitative interpretation of IVIM measurements of vascular perfusion in the rat brain. *Magn. Reson. Med.* **32**, 464–469.

Horton, J. C. & Hedley-White, E. T. 1984 Mapping of cytochrome oxidase patches and ocular dominance columns in human visual cortex. *Phil. Trans. R. Soc. Lond.* B **304**, 255–272.

Horton, J. C., Dagi, L. R. & McCrane, E. P. 1990 Arrangement of ocular dominance columns in human visual cortex. *Arch. Ophthalmol.* **108**, 1025–1031.

Hoult, D. I. & Lauterbur, P. C. 1979 The sensitivity of the zeugmatographic experiment involving human samples. *J. Magn. Reson.* **34**, 425–433.

Hu, X. & Kim, S.-G. 1994 Reduction of physiological noise in functional MRI using navigator echo. *Magn. Reson. Med.* **31**, 495–503.

Hu, X., Le, T. H., Parrish, T. & Erhard, P. 1995 Retrospective estimation and correction of physiological fluctuation in functional MRI. *Magn. Reson. Med.* **34**, 201–212.

Hu, X., Le, T. H. & Uğurbil, K. 1997 Evaluation of the early response in fMRI using short stimulus duration. *Magn. Reson. Med.* **37**, 877–884.

Hubel, D. H. & Wiesel, T. N. 1968 Receptive field and functional architecture of monkey striate cortex. *J. Physiol.* (*Lond.*) **195**, 215–243.

Hubel, D. H. & Wiesel, T. N. 1972 Laminar and columnar distribution of geniculo-cortical fibers in the macaque monkey. *J. Comp. Neurol.* **146**, 421–450.

Hubel, D. H. & Wiesel, T. N. 1977 Functional architechture of macaque monkey visual cortex. *Proc. R. Soc. Lond.* B **198**, 1–59.

Hubel, D. H., Wiesel, N. & Lam, D. M. K. 1974 Autoradiographic demonstration of ocular-dominance columns in the monkey striate cortex by means of transneuronal transport. *Brain Res.* **79**, 273.

Hyde, J. S., Biswal, B., Song, A. W. & Tan, S. G. 1994 Physiological and instrumental fluctuations in fMRI data. In *Second Annual Midwest Functional MRI Workshop*. Madison, WI.

Kennan, R. P., Zhong, J. & Gore, J. C. 1994 Intravascular susceptibility contrast mechanisms in tissue. *Magn. Reson. Med.* **31**, 9–31.

Kennedy, C., Des Rosiers, M. H. & Sakurada, O. 1976 Metabolic maps of the primary visual system of the monkey by means of autoradiographic ^{14}C-deoxyglucose technique. *Proc. Natl Acad. Sci. USA* **73**, 4230–4234.

Kim, S.-G. 1995 Quantification of relative cerebral blood flow change by flow-sensitive alternating inversion recovery (FAIR) technique: application to functional mapping. *Magn. Reson. Med.* **34**, 293–301.

Kim, S.-G. & Richter, W. 1996 Limitations of temporal resolution in fMRI. In *International Society of Magnetic Resonance in Medicine.* New York.

Kim, S.-G. & Tsekos, N. V. 1997 Perfusion imaging by a flow-sensitive alternating inversion recovery (FAIR) technique: application to functional brain imaging. *Magn. Reson. Med.* **37**, 425–435.

Kim, S.-G. & Uğurbil, K. 1997 Comparison of blood oxygenation and cerebral blood flow effects in fMRI: estimation of relative oxygen consumption change. *Magn. Reson. Med.* **38**, 59–65.

Kim, S.-G., Richter, W. & Uğurbil, K. 1997 Limitations of temporal resolution in functional MRI. *Magn. Reson. Med.* **37**, 631–636.

Kleinschmidt, A., Merboldt, K. D., Hanicke, W., Steinmetz, H. & Frahm, J. 1994 Correlational imaging of thalamocortical coupling in the primary visual pathway of the human brain. *J Cerebr. Blood-Flow Metab.* **14**, 952–957.

Kwong, K. K. (and X others) 1992 Dynamic magnetic resonance imaging of human brain activity during primary sensory stimulation. *Proc. Natl Acad. Sci. USA* **89**, 5675–5679.

Kwong, K. K., Chesler, D. A., Weisskoff, R. M., Donahue, K. M., Davis, T. L., Ostergaard, L., Campbell, T. A. & Rosen, B. R. 1995 MR perfusion studies with T1-weighted echo planar imaging. *Magn. Reson. Med.* **34**, 878–887.

Lauterbur, P. C. 1973 Image formation by induced local interaction: examples employing nuclear magnetic resonance. *Nature* **241**, 190–191.

Lee, S.-P., Silva, A. C., Uğurbil, K. & Kim, S.-G. 1999 Diffusion weighted spin-echo fMRI at 9.4 T: microvascular/tissue contribution to BOLD signal changes. (Submitted.)

LeVay, S., Connolly, M. & Houde, J. 1985 The complete pattern of ocular dominance stripes in the striate cortex and visual field of the macaque monkey. *J. Neurosci.* **5**, 486–501.

McIntosh, J., Zhang, Y., Kidambi, S., Harshbarger, T., Pohost, M. G. & Twieg, D. 1996 Echo time dependence of functional MRI 'fast response'. In *Annual Meeting of the International Society of Magnetic Resonance in Medicine*. New York, NY.

Malonek, D. & Grinvald, A. 1996 Interactions between electrical activity and cortical microcirculation revealed by imaging spectroscopy: implication for functional brain mapping. *Science* **272**, 551–554.

Malpeli, J. G. & Baker, F. H. 1975 The representation of the visual field in the lateral geniculate nucleus of *Macaca mulatta*. *J. Comp. Neurol.* **161**, 569–594.

Mandeville, J. B., Marota, J. J. A., Ayata, C., Moskowitz, M., Rosen, B. R. & Weisskoff, R. M. 1998*a* CBV response exhibits 2 phases during rat forepaw stimulation. In *International Society of Magnetic Resonance in Medicine. Sixth Scientific Meeting and Exhibition*. Sydney, Australia.

Mandeville, J. B., Marota, J. J., Kosofsky, B. E., Keltner, J. R., Weissleder, R., Rosen, B. R. & Weisskoff, R. M. 1998*b* Dynamic functional imaging of relative cerebral blood volume during rat forepaw stimulation. *Magn. Reson. Med.* **39**, 615–624.

Menon, R. S., Ogawa, S., Tank, D. W. & Uğurbil, K. 1993 4 tesla gradient recalled echo characteristics of photic stimulation-induced signal changes in the human primary visual cortex. *Magn. Reson. Med.* **30**, 380–386.

Menon, R. S., Hu, X., Adriany, G., Andersen, P., Ogawa, S. & Uğurbil, K. 1994 Comparison of SE-EPI, ASE-EPI and conventional EPI applied to functional neuroimaging: the effect of flow crushing gradients on the BOLD signal. In *Proceedings of the Society of Magnetic Resonance*.

Menon, R. S., Ogawa, S., Hu, X., Strupp, J. P., Anderson, P. & Uğurbil, K. 1995 BOLD based functional MRI at 4 tesla includes a capillary bed contribution: echo-planar imaging correlates with previous optical imaging using intrinsic signals. *Magn. Reson. Med.* **33**, 453–459.

Menon, R. S., Ogawa, S. & Uğurbil, K. 1996 Mapping ocular dominance columns in human V1 using fMRI. *NeuroImage* **3**, S357.

Menon, R. S., Ogawa, S., Strupp, J. P. & Uğurbil, K. 1997 Ocular dominance in human V1 demonstrated by functional magnetic resonance imaging. *J. Neurophysiol.* **77**, 2780–2787.

Menon, R. S., Luknowsky, D. C. & Gati, J. S. 1998 Mental chronometry using latency-resolved functional MRI. *Proc. Natl Acad. Sci. USA* **95**, 10 902–10 907.

Mitra, P. P., Thompson, D. J., Ogawa, S., Hu, X. & Uğurbil, K. 1995 Spatio-temporal patterns in fMRI data revealed by principal component analysis and subsequent low pass filtering. In *Third Scientific Meeting of the Society of Magnetic Resonance*. Nice, France.

Mitra, P. P., Ogawa, S., Hu, X. & Uğurbil, K. 1997 The nature of spatio-temporal changes in cerebral hemodynamics as manifested in functional magnetic resonance imaging. *Magn. Reson. Med.* **37**, 511–518.

Moore, G. G., Zhang, Y. T. & Twieg, D. B. 1997 Assessment of the fast response spatial distribution. In *International Society of Magnetic Resonance in Medicine. Fifth Scientific Meeting and Exhibition*. Vancouver, British Columbia.

Nolte, J. 1993 *The human brain, an introduction to its functional anatomy*, 3rd edn. St Louis: Mosby Year Book.

Ogawa, S. & Lee, T.-M. 1990 Magnetic resonance imaging of blood vessels at high fields: *in vivo* and *in vitro* measurements and image simulation. *Magn. Reson. Med.* **16**, 9–18.

Ogawa, S., Lee, T.-M., Kay, A. R. & Tank, D. W. 1990*a* Brain magnetic resonance imaging with contrast dependent on blood oxygenation. *Proc. Natl Acad. Sci. USA* **87**, 9868–9872.

Ogawa, S., Lee, T.-M., Nayak, A. S. & Glynn, P. 1990*b* Oxygenation-sensitive contrast in magnetic resonance image of rodent brain at high magnetic fields. *Magn. Reson. Med.* **14**, 68–78.

Ogawa, S., Tank, D. W., Menon, R., Ellermann, J. M., Kim, S.-G., Merkle, H. & Ugurbil, K. 1992 Intrinsic signal changes accompanying sensory stimulation: functional brain mapping with magnetic resonance imaging. *Proc. Natl Acad. Sci. USA* **89**, 5951–5955.

Ogawa, S., Menon, R. S., Tank, D. W., Kim, S.-G., Merkle, H., Ellermann, J. M. & Uğurbil, K. 1993 Functional brain mapping by blood oxygenation level-dependent contrast magnetic resonance imaging. *Biophys. J.* **64**, 800–812.

Ogawa, S., Mitra, P. P., Hu, X. & Uğurbil, K. 1996 Spatio-temporal patterns revealed in denoised fMRI data. Visualization of information processing in the human brain. In *Recent advances in MEG and functional MRI* (ed. I. Hashimoto, Y. C. Okada & S. Ogawa), pp. 5–14.

Ogawa, S., Menon, R. S., Kim, S.-G. & Uğurbil, K. 1998 On the characteristics of functional magnetic resonance imaging of the brain. *A. Rev. Biophys. Biomol. Struct.* **27**, 447–474.

Ogren, M. & Hendrickson, A. 1976 Pathways between striate cortex and subcortical regions in *Macaca mulatta* and *Saimiri sciureus*: evidence for a reciprocal pulvinar connection. *Exp. Neurol.* **53**, 780–800.

Purcell, E. M., Torrey, H. C. & Pound, R. V. 1945 Resonance absorbtion by nuclear magnetic moments in a solid. *Phys. Rev.* **69**, 37–38.

Rabi, I. I., Zacharias, J. R., Millman, S. & Kusch, P. 1938 A new method of measuring nuclear magnetic moment. *Phys. Rev.* **53**, 318.

Rabi, I. I., Millman, S. & Kusch, P. 1939 The molecular beam resonance method for measuring nuclear magnetic moments. *Phys. Rev.* **55**, 526–535.

Raichle, M. E. 1987 Circulatory and metabolic correlates of brain function in normal humans. In *Handbook of physiology—the nervous system*, pp. 643–674.

Rakic, P. 1976 Prenatal genesis of connections subserving ocular dominance in the rhesus monkey. *Nature* **261**, 467–471.

Rezak, M. & Benevento, L. A. 1979 A comparison of the organization of the projections of the dorsal lateral geniculate nucleus, the inferior pulvinar and adjacent lateral pulvinar to primary visual cortex (area 17) in the macaque monkey. *Brain Res.* **167**, 19–40.

Richter, W. & Kim, S.-G. 1996 Temporally resolved human brain activity of delayed cued finger movements studied by fMRI. In *Society of Neuroscience*. Washington, DC.

Richter, W., Uğurbil, K. & Kim, S.-G. 1996 Limitation of temporal resolution in fMRI. *NeuroImage* **3**, S38.

Richter, W., Andersen, P. M., Georgopoulos, A. P. & Kim, S.-G. 1997*a* Sequential activity in human motor areas during a delayed cued finger movement task studied by time-resolved fMRI. *NeuroReport* **8**, 1257–1261.

Richter, W., Uğurbil, K., Georgopoulos, A. P. & Kim, S.-G. 1997*b* Time-resolved fMRI of mental rotation. *NeuroReport* **8**, 3697–3702.

Richter, W., Georgopoulos, A. P., Uğurbil, K. & Kim, S.-G. 1997*c* Detection of brain activity during mental rotation in a single trial by FMRI. In *International Society of Magnetic Resonance in Medicine*.

Roberts, D. A., Detre, J. A., Bolinger, L., Insko, E. K. & Leigh, J. S. 1994 Quantitative magnetic resonance imaging of human brain perfusion at 1.5T using steady-state inversion of arterial water. *Proc. Natl Acad. Sci. USA* **91**, 33–37.

Robinson, D. L. & Petersen, S. E. 1992 The pulvinar and visual salience. *Trends Neurosci.* **15**, 127–132.

Savoy, R. L., Gandettini, P. A., O'Craven, K. M., Kwong, K. K., Davis, T. L., Baker, J. R., Bellieau, J. W., Weisskoff, R. M. & Rosen, B. R. 1995 Pushing the temporal resolution of fMRI: studies of very brief visual stimuli, onset variability and asynchrony, and stimulus-correlated changes in noise. In *Third Scientific Meeting of the Society of Magnetic Resonance in Medicine*. Nice, France.

Schiller, P. H., Logothetis, N. K. & Charles, E. R. 1990*a* Role of the color-opponent and broad-band channels in vision. *Vis. Neurosci.* **5**, 321–346.

Schiller, P. H., Logothetis, N. K. & Charles, E. R. 1990*b* Functions of the colour-opponent and broad-band channels of the visual system [see comments]. *Nature* **343**, 68–70.

Sereno, M. I., Dale, A. M., Reppas, J. B., Kwong, K. K., Belliveau, J. W., Brady, T. J., Rosen, B. R. & Tootell, R. B. H. 1995 Borders of multiple visual areas in humans revealed by functional magnetic resonance imaging. *Science* **268**, 889–893.

Shepard, R. N. & Metzler, J. 1971 Mental rotation of three-dimensional objects. *Science* **171**, 701–703.

Song, A. W., Wong, E. C., Tan, S. G. & Hyde, J. S. 1996 Diffusion weighted fMRI at 1.5 T. *Magn. Reson. Med.* **35**, 155–158.

Stejskal, E. O. & Tanner, J. E. 1965 Spin diffusion measurements: spin-echoes in the presence of a time dependent field gradient. *J. Chem. Phys.* **42**, 288–292.

Thulborn, K. R., Waterton, J. C., Mattews, P. M. & Radda, G. K. 1982 Oxygenation dependence of the transverse relaxation time of water protons in whole blood at high field. *Biochem. Biophys. Acta* **714**, 265–270.

Thulborn, K. R., Waterton, J. C. & Matthews, P. M. 1992 Dependence of the transverse relaxation time of water protons in whole blood at high field. *Biochem. Biophys. Acta* **714**, 265–272.

Ts'o, D. Y., Frostig, R. D., Lieke, E. E. & Grinvald, A. 1990 Functional organization of primate visual cortex revealed by high resolution optical imaging. *Science* **249**, 417–420.

Tuong, H. L. & Hu, X. 1996 Evaluation of the early response in fMRI in individual subjects using short stimulus duration. In *Proceedings of the International Society of Magnetic Resonance in Medicine*. New York, NY.

Twieg, D. B., Moore, G. G., Zhang, Y. T. & X. Estimating fast response onset time. In *International Society of Magnetic Resonance in Medicine. Fifth Scientific Meeting and Exhibition*. Vancouver, British Columbia.

Van Zijl, P. C., Eleff, S. M., Ulatowski, J. A., Oja, J. M., Ulug, A. M., Traystman, R. J. & Kauppinen, R. A. 1998 Quantitative assessment of blood flow, blood volume and blood oxygenation effects in functional magnetic resonance imaging [see comments]. *Nature Med.* **4**, 159–167.

Weisskoff, R. M., Boxerman, J. L., Zuo, C. S. & Rosen, B. R. 1993 Endogenous susceptibility contrast: principles of relationship between blood oxygenation and MR signal change. In *Functional MRI of the brain*. Arlington, VA.

Weisskoff, R. M., Zuo, C. S., Boxerman, J. L. & Rosen, B. R. 1994 Microscopic susceptibility variation and transverse relaxation: theory and experiment. *Magn. Reson. Med.* **31**, 601–610.

Wong, E. C., Buxton, R. B. & Frank, L. R. 1998 Quantitative imaging of perfusion using a single subtraction (QUIPSS and QUIPSS II). *Magn. Reson. Med.* **39**, 702–708.

Zeki, S. 1993 *A vision of the brain*. Blackwell Scientific Publications.